THE TULU KAPI GOLD DEPOSIT OF THE WESTERN ETHIOPIAN SHIELD: STRUCTURAL FRAMEWORK, U-PB ZIRCON GEOCHRONOLOGY AND PARAGENESIS

by

Zsolt B. K. Molnar

A thesis
presented to the University of Waterloo
in fulfillment of the
thesis requirement for the degree of
Master of Science
in
Geology

Waterloo, Ontario, Canada, 2019

AUTHOR'S DECLARATION

This thesis consists of material all of which I authored or co-authored: see Statement of Contributions included in the thesis. This is a true copy of the thesis, including any required final revisions, as accepted by my examiners.

I understand that my thesis may be made electronically available to the public.

Statement of Contributions

Significant contributions were made to section 2.6, U-Pb Geochronology, by Professor Chris Yakymchuk.

For the U-Pb age dating, Professor Chris Yakymchuk collected and reduced the data and I chose the analytical spots and helped interpret the data.

Abstract

Gold production dates back millennia in the Arabian Nubian Shield. Most of the mined deposits are in the northern portions of the shield, with little know about its southern extent. Tulu Kapi is a rare example of a gold deposit in the southern Arabian Nubian Shield. Tulu Kapi is located in a greenstone belt, whose central feature is the transcontinental Tuludimtu shear zone, in the Western Ethiopian Shield. U–Pb zircon geochronology indicates that the Tulu Kapi deposit is hosted by the 738 ± 2.6 Ma Tulu Kapi syenite, which is juxtaposed against the 699 ± 2.7 Ma Kapi Gabbro. Both intrusions are bordered by the Bedele shear zone to the east, which is a splay off the Tuludimtu shear zone. The Tulu Kapi syenite is host to brittle structures as which contrasts the surrounding volcanic and sedimentary rocks, which are relatively the ductile. Gold mineralization and alteration are found throughout the Tulu Kapi syenite in en-echelon vein arrays and related structures, which are controlled by conjugate shear zones in the syenite.

The most intensely deformed area of the gold deposit takes the form a plunging shoot at the footwall of the syenite. The shoot consists of superimposed brittle structures found at a three-way contact. Intense alteration, veining and gold mineralization are indicative of the shoot's role as a crucial fluid pathway in the deposit. In the centre of the deposit, the shoot intersects a dyke swarm where the focused fluid pathway disperses into the en-echelon vein arrays and adjoining structures which network through the syenite forming the gold deposit.

Acknowledgements

I thank the community around the project area for their help in the field and land access during this study. Additionally, I thank KEFI Minerals Plc. for the funding of this thesis and KEFI Minerals Ethiopia Plc. and its staff for logistical support during the course of this study.

I thank my thesis supervisors Shoufa Lin and Chris Yakymchuk for their technical and articulation guidance, as well as their encouragement during the course of this MSc thesis project. I am also grateful to my committee for their useful feedback: Shoufa Lin, Chris Yakymchuk, Brian Kendall and Cees Van Staal.

I thank Simon Cleghorn, formerly of KEFI Minerals Plc., for his commitment to supporting this MSc study.

Also, I thank the many people at the University of Waterloo who supported me technically and logistically throughout this project and those who encouraged me.

Three-dimensional modelling of the Tulu Kapi lodes and northern and southern dyke swarms was carried out by the author (Molnar) during his employment with Nyota Minerals in 2012 and KEFI Minerals Ltd., in 2014 and 2015.

Finally, I thank my wife, Mercy, for her consistent support.

Dedication

I dedicate my thesis to my wife, Mercy.

Table of Contents

List of Figures

List of Tables

Chapter 1 Introduction

1.1 Project location

The Tulu Kapi gold deposit is located in western Ethiopia, 350 km due west from the capital of Addis Ababa. Tulu Kapi is found in the Western Ethiopian Shield (WES) which is one of the western-most exposures of the Neoproterozoic Arabian Nubian Shield (ANS) (Figure 1-1).

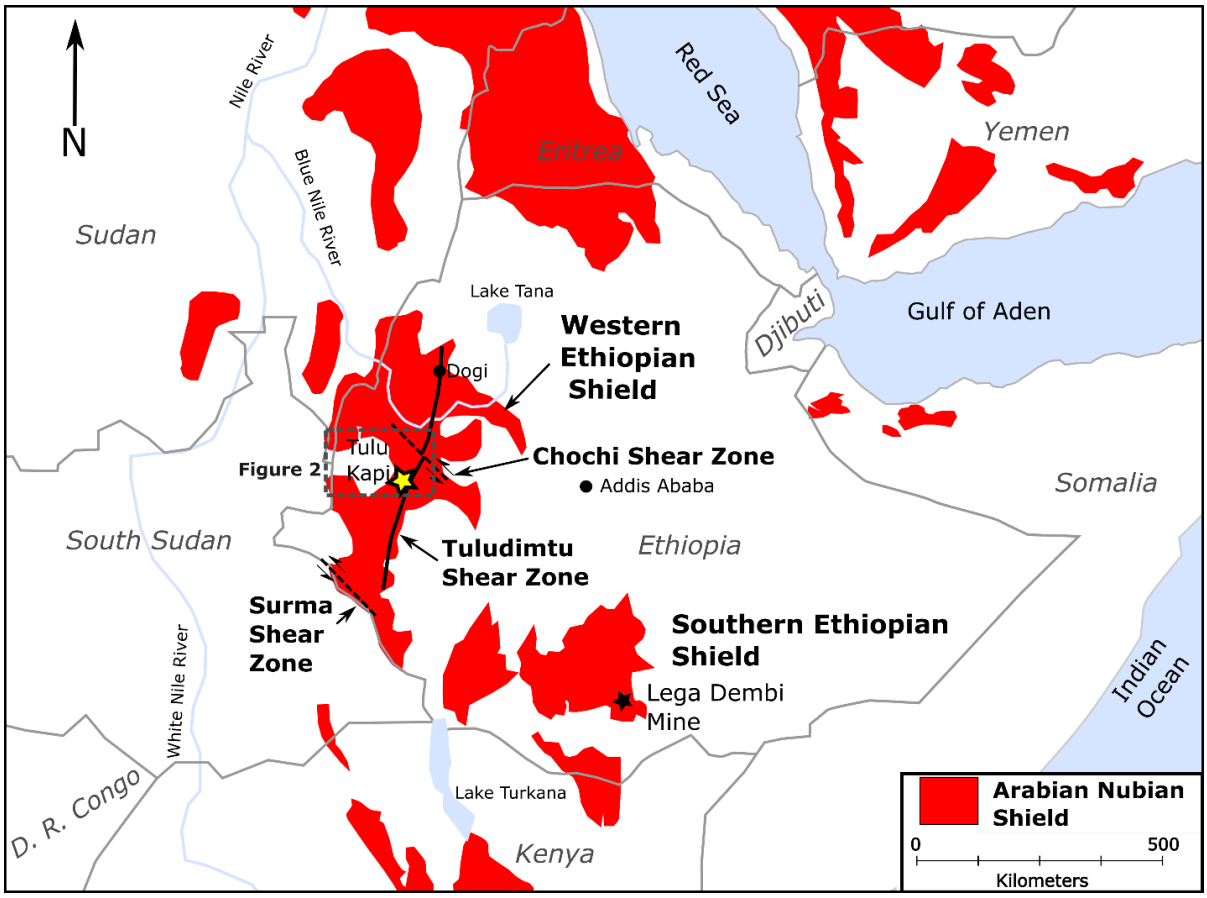

Figure 1-1: The Arabian Nubian Shield and the Tuludimtu shear zone (After Fritz et al., 2013).

1.2 Tulu Kapi mining and exploration history

Gold production in the ANS dates to pre-historic times, with an estimated one-hundred million ounces mined (Goldfarb et al., 2001; Johnson et al, 2017). Today, gold is mined in Egypt, Sudan, the Kingdom of Saudi Arabia, Eritrea and Ethiopia (Johnson et al, 2017). Most previous economic

geological studies in the Arabian Nubian Shield have focused on the northern portion of the shield: Egypt, Sudan, Kingdom of Saudi Arabia and Eritrea (Johnson et al. 2017), where known gold deposits are concentrated. The southern portion of the ANS, made up of the WES and the Southern Ethiopian Shield (Figure 1-1), has received much less attention. The shear zone hosted Lege Dembi Mine in the Adola Belt of the Southern Ethiopian Shield (Worku, 1996) is the only large-scale gold operation in the southern ANS (Figure 1-1). The greenschist facies orogenic belts and trans-continental shear zones which cut across the ANS in Ethiopia appear to be analogous to globally typical host sites for orogenic gold deposits. The single large-scale mine may only reflect the minimal work done in the southern ANS.

The WES has no record of primary gold mining, only alluvial workings. This is possibly due to difficulty of access as well as saprolite and regolith cover complicating gold exploration. One of the few documented gold deposits in the WES is Tulu Kapi. Therefore, understanding the genesis of the Tulu Kapi deposit is crucial for gold exploration models in the WES.

While gold extraction in the ANS dates back millennia, records of mining are not readily available, particularly in the southern ANS which includes the WES. The first recorded mining activities carried out in the WES, including Tulu Kapi, was by Fascist Italy during the 6-year annexation of Ethiopia, which ended in 1941 (Granitzio et al, 2017). During their occupation of Ethiopia, SAPIE, a Fascist Italian government organized mining firm, undertook exploration and alluvial mining activities at Tulu Kapi.

Subsequent to the colonial era, exploration activities in Tulu Kapi were carried out by the Geological Survey of Ethiopia and the United Nations Development Program from 1969-1972, Tan-Range Resources from 1996-1998, Golden Prospect Mining Company from 2005-2009, Nyota Minerals Pty. From 2009 to 2013 and KEFI Minerals Ltd from 2014 to the present day (Granitzio et al, 2017).

1.3 Geological setting

1.3.1 Arabian Nubian Shield

The ANS consists of amalgamated arcs and is a product of the East African Orogen orogenic cycle (Stern, 1994). The cycle began with the breakup of Rodinia (870-800 Ma), which led to the formation of the Mozambique Ocean. Subduction in the Mozambique Ocean led to island-arc formation and accretion of arc terranes. The cycle culminated with the amalgamation of east and west Gondwana (650-600 Ma) (Johnson et al, 2011; Stern, 1994). The northern part of the East African Orogeny is made up of the oceanic affinity ANS and the southern part is made up of the higher metamorphic grade Mozambique Mobile Belt (Johnson et al, 2011; Stern, 1994).

1.3.2 Western Ethiopian Shield

The WES is a part of the ANS (Figure 1-1). The tectonic evolution of the WES is generally the same as the East African Orogeny, which includes early rifting, associated sedimentation, subduction and island-arc formation, and protracted continent-continent collision (Johnson et al, 2004). Interpretations of the linear belts of deformed mafic-ultramafic bodies with the ANS vary between ophiolites marking a suture zone and intrusive rocks marking extensional arc/back-arc setting or Alaskan type ultramafic intrusion of an island arc setting (Blades et al, 2015 and references therein).

1.4 Prior structural analysis

1.4.1 Western Ethiopian Shield

East-west shortening has been recorded throughout the WES; these structures typically strike north-south and dip steeply east and west (Johnson et al, 2004). The pervasive, steep north-south structural trend supports east-west sub-horizontal shortening. The more commonly eastward-dip of structures and sub-horizontal fold axes advocate westerly directed bulk transport and thrusting (Allen and Tadesse, 2004; Johnson et al, 2004). Following the westerly directed thrusting, sinistral shear zones developed, at times reactivating thrusts (Johnson et al, 2004), like at Baruda (Braathen et al., 2001). Steeply eastward dipping thrusts concentrate at domain boundaries, like at the margin of the Tuludimtu ultramafic belt – this suggests that most of the shortening was taken up in these areas (Johnson et al, 2004).

The WES can be divided into five lithotectonic domains (Allen and Tadesse, 2003); from east to west: Didesa, Kemashi, Dengi, Sirkole and Daka (Figure 1-2). The Tulu Kapi deposit is hosted in the Kemashi domain, which consists of low-grade metasedimentary and ultramafic-mafic metavolcanic rocks intruded by ultramafic to intermediate plutons (Allen and Tadesse, 2003; Alemu and Abebe, 2007). The intruding plutons include the deformed Tulu Kapi syenite (Kebede et al., 1999) and the un-deformed Genji granite (Figure 1-2) with a $^{206}Pb/^{238}U$ zircon age of 584±10 Ma (Blades et al., 2015). The Tuludimtu shear zone is the central feature of the WES (Figure 1-1), along which the Tulu Kapi syenite is found.

1.4.2 Tuludimtu shear zone

The Tuludimtu shear zone is central to a north-northeast trending fold and thrust belt (Alemu and Abebe, 2007).

Three deformation episodes were identified along the Tuludimtu shear zone in metavolcanics rocks of the Kemashi domain by Allen and Tadesse (2003). The first is east-west shortening with related thrusting. The second, still in an east-west compressional regime, was the development of northwest-southeast strike slip structures and folding in less competent lithologies. Finally, brittle-ductile strike-slip reactivation of the Chochi shear zone and possibly others, which caused sinistral offsetting of domain boundaries (Figure 1-2). Gold and base metal mineralization along the Chochi shear zone may have been related to this event (Allen and Tadesse, 2003). These events, which Allen and Tadesse (2003) break up into three progressive deformation stages, are thought to have manifested during protracted east-west compression when terranes and continents were colliding during the East African Orogeny to form Gondwana (Johnson et al, 2011).

Two deformation events are documented by Braathen et al (2001) in the Baruda shear zone, ~120 km north of Tulu Kapi. The Baruda shear zone is the local name for the Tuludimtu shear zone north of the Chochi shear zone. The first deformation event is indicated to be top-to-the-west by shear sense indicators. Foliation is north-south to northeast-southwest striking and steeply dipping, while lineation is steeply plunging. The second deformation event' structures are L-S tectonized shear zones that strike north-northeast to south-southwest and north to south near Baruda; the lineation is sub-horizontal north-south. Some early high strain zones are reactivated by this later event. Along the margins of mechanically stronger rocks, this late deformation is brittle.

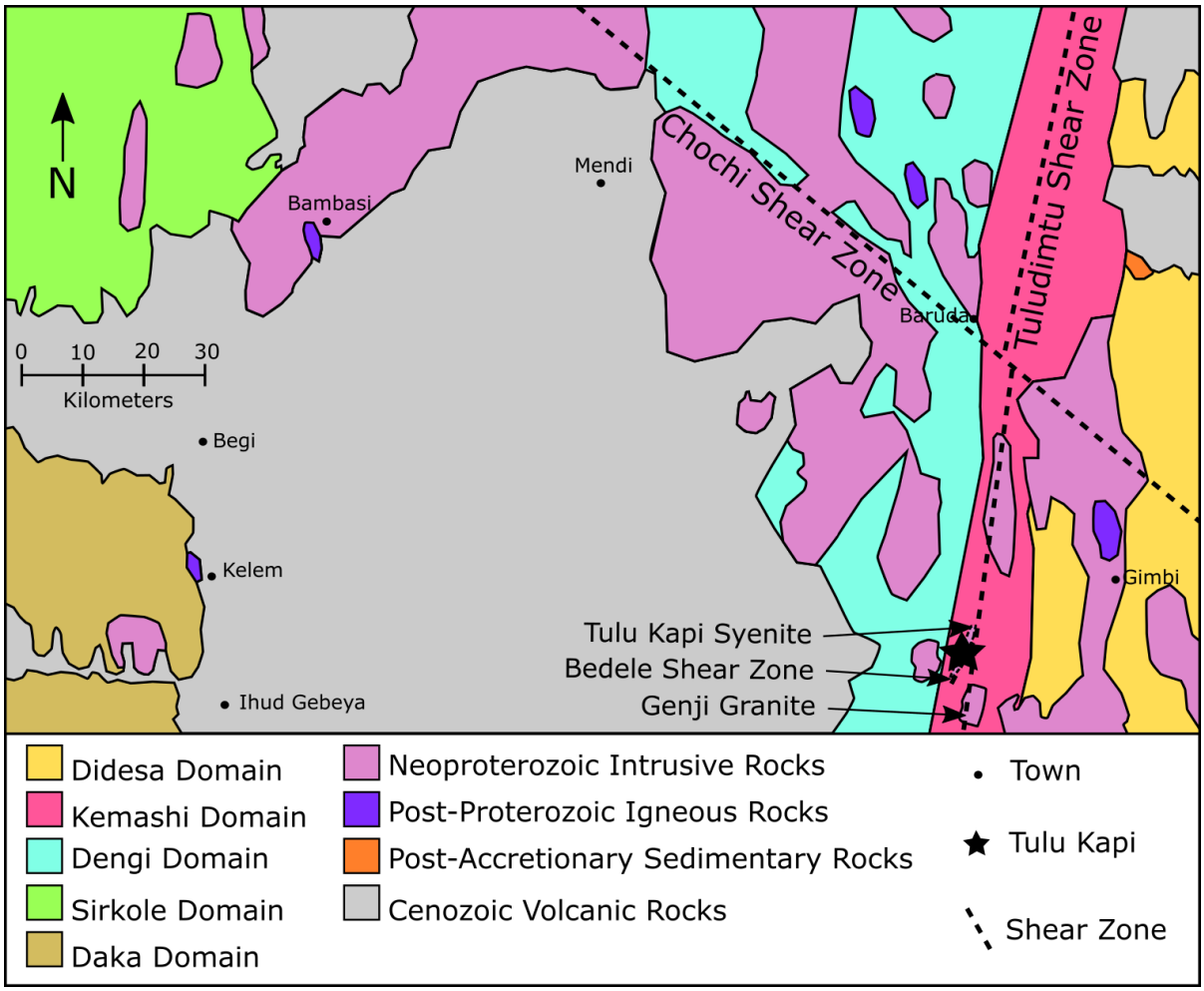

Figure 1-2: Domain map of the Western Ethiopian Shield (modified after Allen and Tadesse, 2003, and Blades et al., 2015). The star is the location of Figure 2-1.

Extensional deformation is not documented in the WES aside from the work of Yihunie et al. (2007). Sub-horizontal normal-slip structures along the Tuludimtu shear zone have been interpreted to represent gravitational collapse towards the end of orogenesis (Yihunie et al. 2007).

1.4.3 Tulu Kapi specific work

Kebede et al (1999) is the only worker to have published on the Tulu Kapi syenite. The Tulu Kapi syenite is inferred to be the result of partial melting of source rocks enriched in high field strength

elements, and is a typical A-type granite (Kebede et al., 1999). Its close association with the Tuludimtu shear zone may suggest that the pluton rose along the deep-rooted fault structure. Kebede et al. (1999) suggested that the Tulu Kapi syenite was post tectonic.

1.5 Metamorphism

Two regional metamorphic events are documented in the WES (Ayalew et al 1990, Johnson et al 2004). The ages of these events are 800-770 Ma, which reached amphibolite facies, and 635-580Ma, which is interpreted to be lower temperature than the first metamorphic event, however its P-T conditions have been problematic to determine (Johnson et al, 2004). Folded leucosomes associated with east-west shortening in anatectic migmatites suggest that the first metamorphic event predates east-west shortening-driven tectonism (Johnson et al, 2004). The overprinting of late transpression-related structures suggest that the second metamorphic event ended after the final accretion of the ANS (Johnson et al, 2004). Johnson et al (2004) report that the second metamorphic event is restricted to the Tuludimtu shear zone-proximate domains and is not found in the flanking gneissic Daka, Sirkole and Didesa domains (Figure 1-2), suggesting that it was fluid driven.

Abundantly widespread chlorite, talc and muscovite-rich rocks imply that greenschist-facies metamorphism occurred throughout most of the Kemashi and Dengi domains, although rare lower amphibolite conditions can be found (Johnson et al, 2004). Thermobarometry of a sample from the Kemashi domain yielded 570 ± 11 °C and 8.6 ± 2.2 kbar (Johnson et al, 2004). Tadesse and Allen (2004) document significant metamorphic alteration proximate to the Tuludimtu shear zone as opposed to distal, implying higher volumes of fluid flux.

1.6 Research questions and approach

The purpose of this thesis is to define the structural framework of the Tulu Kapi gold deposit and to develop the understanding of the structural and temporal controls on gold mineralization in the WES.

The thesis addresses the following questions:

1. What are controls on mineralization in the Tulu Kapi gold deposit?
2. What are the absolute and relative time constraints on gold mineralization in Tulu Kapi?

These questions are addressed through structural analysis of outcrop and oriented diamond drill core including field relationships, U-Pb geochronology and petrography of regular and polished thin sections.

The structural model developed during the course of this thesis was applied to an existing Tulu Kapi mineralization model (KEFI Minerals Plc., 2015), which was built by the author in January 2015 in Datamine Studio 3 mining software, to test it for consistency.

U-Pb ages of the Tulu Kapi syenite and Kapi gabbro from this research along with the work of Blades et al. (2015) are used as absolute constraints on gold mineralization in Tulu Kapi. This constraint is inferred for plutons along the Tuludimtu shear zone. The LA-ICP-MS results are available in Appendix A.

Thin section petrography is used in this paper to describe the gold hosting lithologies of the Tulu Kapi gold deposit, while polished section analyses are used to infer a paragenetic sequence for gold and ore minerals in Tulu Kapi.

Lithogeochemical analysis was carried out at Actlabs in Ontario, Canada, on all nine U-Pb samples (Table 1-1-1). The results of the analysis are not used in this thesis due to the samples being too few to make solid statements on the evolution of the Tulu Kapi syenite's melt source. The results of the analyses are presented in Appendix B.

Table 1-1-1: U-Pb and lithogeochemistry analyses sample summary table.

Sample ID	Rock Field Name	Source of sample
D01	Quartz syenite	Outcrop
D02	Metavolcanic	Outcrop
D03	Albitized syenite	Diamond drill-core
D04	Type-I dyke	Diamond drill-core
D05	Tulu Kapi syenite	Diamond drill-core
D06	Kapi Gabbro	Diamond drill-core
D07	Footwall volcanic	Diamond drill-core
D08	Type-III dyke	Diamond drill-core
D09	Type-II dyke	Diamond drill-core

Chapter 2 Tulu Kapi Gold Deposit, Western Ethiopian Shield: Structural framework, U-Pb zircon geochronology and paragenesis

2.1 Introduction

Gold production in the Arabian Nubian Shield (ANS) dates to pre-historic times, with an estimated one-hundred million ounces mined (Goldfarb et al., 2001; Johnson et al., 2017). Today, gold is mined in Egypt, Sudan, the Kingdom of Saudi Arabia, Eritrea and Ethiopia (Johnson et al., 2017). Previous studies of gold mineralization in the Arabian Nubian Shield have focussed on the northern portion of the shield where known gold deposits are concentrated. The southern portion of the ANS, made up of the Western Ethiopian Shield (WES) and the Southern Ethiopian Shield (Figure 1-1), has received much less attention. The shear zone hosted Lege Dembi Mine in the Adola Belt of the Southern Ethiopian Shield (Ghebreab et al., 1992; Worku, 1996) is the only large-scale gold operation in the southern ANS. Greenschist-facies orogenic belts and trans-continental shear zones that cut across the ANS in Ethiopia appear to be analogous to settings for structurally-controlled orogenic gold deposits around the world. Therefore, there is good geological potential for additional gold deposits in the southern ANS.

Unlike the Southern Ethiopian Shield, the WES has no record of primary gold mining, but only alluvial workings. This is probably due to the difficulty of access as well as extensive saprolite and regolith cover that complicates gold exploration. One of the few documented gold deposits in the WES is Tulu Kapi. An understanding of the genesis of the Tulu Kapi deposit is thus crucial for gold exploration models in the WES.

In this contribution, structural analysis of outcrops and oriented diamond drill core are combined with three-dimensional modelling to generate a macro-scale model of gold hosting structures. Field relationships, ore mineral petrology and geochronology are used to constrain the timing and nature of gold mineralization at Tulu Kapi. Finally, a genetic model is presented that can be used to explore for greenstone-hosted gold deposits along regional-scale structures in the WES.

2.2 Regional Geology

2.2.1 Arabian Nubian Shield (ANS)

The ANS is located at the northern end of the East African Orogeny (Stern, 1994). Neoproterozoic orogenesis was preceded by the closing of the Mozambique Ocean between 650 and 600 Ma during the formation of Gondwana (Stern, 1994; Johnson et al., 2004; Johnson et al., 2011; Fritz et al., 2013). The southern ANS is exposed in Ethiopia, Kenya and Sudan as the outcropping Southern and Western Ethiopian Shields (Figure 1-1).

2.2.2 The Western Ethiopian Shield

The WES experienced crustal thickening during protracted continental collision where folding and west directed thrusting along existing N-S trending faults dominated (Braathen et al., 2001; Allen and Tadesse, 2004; Johnson et al., 2004; Fritz et al., 2013). Continental collision culminated with oblique collisions in the northeastern Arabian Nubian Shield (Ayalew and Pecerillo, 1998; Fritz et al, 2013). Thrust faults are off-set by northwest trending strike-slip faults, the most notable fault in the Kemashi domain is the sinistral Chochi Shear Zone (Braathen et al, 2001; Allen and Tadesse, 2003; Johnson et al, 2004). Tectonic escape and orogenic collapse mark the final deformation event (Yihunie and Hailu, 2007). This sequence of events, crustal thickening, strike-slip movement and collapse is typical for gold hosting metamorphic belts like the ones found in Australia and Canada (Groves et al., 2000; Robert and Poulsen, 2001; Goldfarb et al., 2005).

The WES can be divided into five lithotectonic domains (Allen and Tadesse, 2003); from east to west: Didesa, Kemashi, Dengi, Sirkole and Daka (Figure 1-2). The Tulu Kapi deposit is hosted in the Kemashi domain, which consist of low-grade metasedimentary and ultramafic-mafic metavolcanic rocks intruded by ultramafic to intermediate plutons (Allen and Tadesse, 2003; Alemu and Abebe, 2007). The intruding plutons include the deformed Tulu Kapi syenite (Kebede et al., 1999) and the un-deformed Genji granite (Figure 1-2) with a $^{206}Pb/^{238}U$ age of 584±10 Ma (Blades et al., 2015). The Tuludimtu shear zone is the central feature of the WES (Figure 1-1), along which the Tulu Kapi syenite is found.

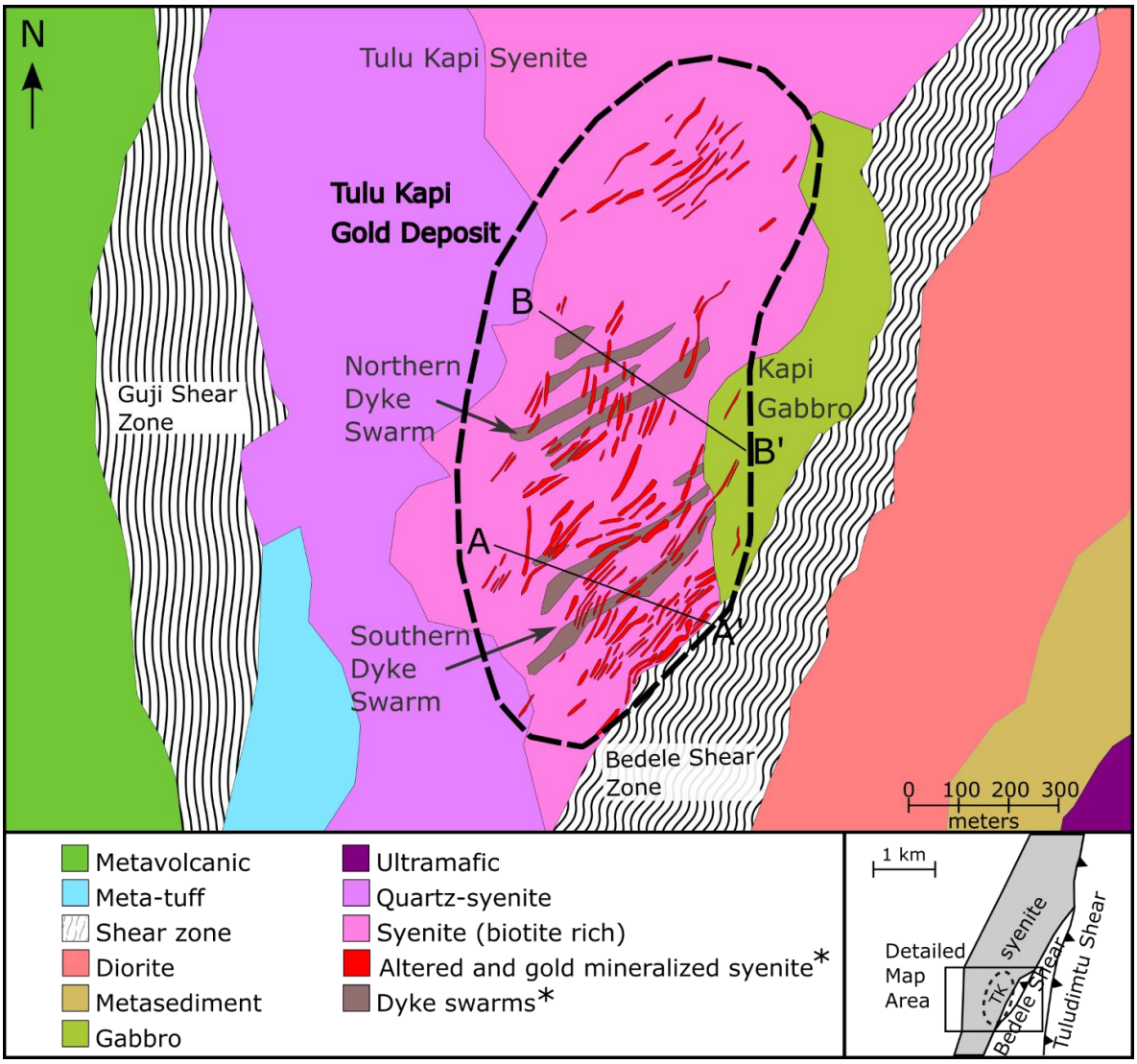

Figure 2-1:Local map of Tulu Kapi (TK), (modified after KEFI Minerals Ltd. DFS, 2015). * Dyke swarms and altered and gold mineralized syenite models are from historical models (KEFI Minerals Ltd. DFS, 2015). A-A' and B-B' are the locations of cross sections for Figure 2-10.

Two regional metamorphic events have been documented in the WES. The ages are 800-770 Ma for M_1, which reached amphibolite-facies, and 635-580 Ma for M_2, which was a lower temperature event than M_1 (Ayalew at al., 1990). The establishment of constraints on P-T conditions for M_2 are reported to have been problematic by Johnson et al. (2004), however, abundantly widespread chlorite,

talc and muscovite-rich rocks imply that greenschist-facies metamorphism occurred throughout most of the Kemashi and Dengi domains, although rare lower amphibolite conditions can be found (Johnson et al, 2004).

2.3 Geology of the Tulu Kapi Deposit Geology

The Tulu Kapi gold deposit is hosted by the Tulu Kapi syenite pluton with minor gold mineralization hosted in the Kapi gabbro to its east. The plutons are bordered by the Bedele shear zone to the southeast and the Guji shear zone to the west (Figure 2-1). The Bedele shear zone, found on the southeast of the deposit, is interpreted to join the Tuludimtu shear zone a few kilometres to the north of Tulu Kapi (Figure 1-2 and Figure 2-1).

2.3.1 Lithology

2.3.1.1 Tulu Kapi Syenite

The Tulu Kapi syenite lies on the west side of the Tuludimtu shear zone and in the hanging-wall of its splay-fault, the Bedele shear zone (Figure 2-1). Quartz veins are found throughout the syenite and are consistent with brittle behaviour during deformation. The margin of the syenite is intensely sheared where in contact with the Bedele shear zone.

The syenite pluton is composed of perthitic K-feldspar, biotite and minor quartz (**Error! Reference source not found.**, A). Typical grain size in the syenite is sub-centimetre; occasional Rapakivi type texture (c.f. Vernon, 2016) has been observed. These textures are overprinted by alteration, which strengthens with proximity to the Bedele shear zone. Chlorite is found throughout the syenite as well as in fractures and as selvages in veins.

2.3.1.2 Kapi Gabbro

The Kapi gabbro occurs immediately to the east of the Tulu Kapi syenite (Figure 2-1). The gabbro consists of plagioclase, clinopyroxene hornblende and biotite. Plagioclase ranges from sub-cm to 5 cm in size, and texture varies from euhedral for the largest crystals to sub-cm sized anhedral plagioclase grains with irregular boundaries. Chlorite is found throughout the gabbro. The contact

between the gabbro and syenite appears to be intrusive, but with some shearing or detachment with proximity to the Bedele shear zone (Figure 2-1).

2.3.1.3 Volcanic Rocks

An assortment of volcanic rocks mostly comprised of trachyte, polymictic conglomerate and quartz-phyric rhyolite form the footwall to the Tulu Kapi syenite. However, the volcanic rocks are not found under the syenite at the southwestern portion of the deposit, presumably due to faulting. The volcanic rocks are cross cut by syenitic dykes and a similar suite of dykes as the Tulu Kapi syenite. From the three-dimensional modelling of drill core data, the footwall of the syenite dips 23° towards 005°. The contact between the volcanic rocks and the Tulu Kapi syenite is tectonic.

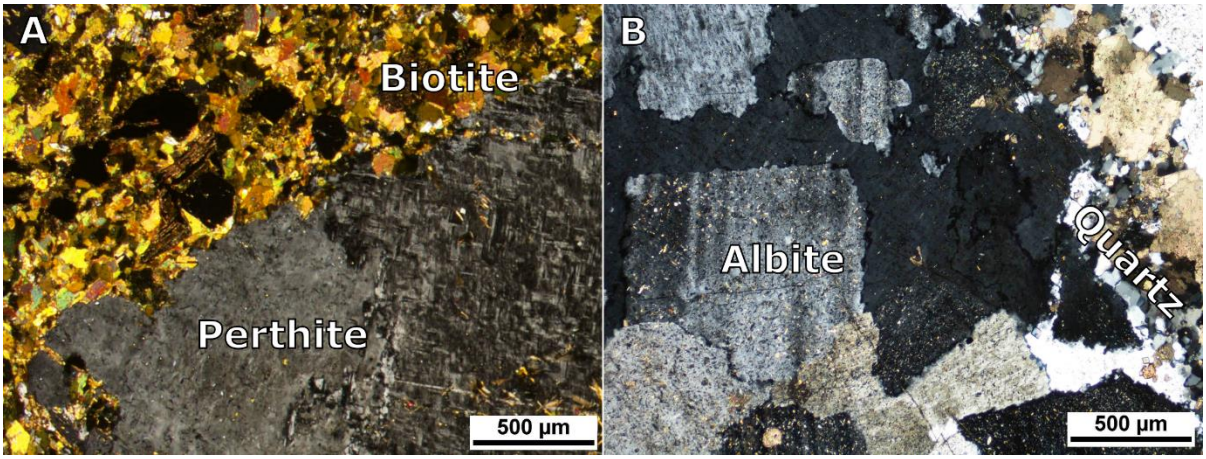

Figure 2-2: (A) Photomicrograph of the syenite in cross-polarized light; (B) Ab + Si + Su altered syenite in cross-polarized light.

2.3.1.4 Dykes and Dyke Swarms

Three dominant dyke types are found in the Tulu Kapi syenite and Kapi gabbro. In interpreted order from early to late intrusion the dykes are:

Type-I: Porphyritic microsyenite;

Type-II: Microsyenogabbro;

Type-III: Microsyenodiorite.

Type-I dykes are aphanitic and contain potassium feldspar, which occur as coarser-grained phenocrysts in the fine-grained matrix. Type-II dykes are fine grained to aphanitic and typically exhibit shear foliation parallel to their contacts with wallrock. Ab + Si + Su (albite + silica + sulfide) altered syenite lodes can be found adjacent to them. Whereas type-I and II dykes are found throughout the Tulu Kapi deposit, there are two distinct clusters of types-I and II dykes, the southern and northern dyke swarms (Figure 2-1). Type-III dykes are aphanitic and most frequently found proximal to the contact between the Tulu Kapi syenite and Bedele shear zone. The dykes cross-cut Ab + Si + Su alteration zones (Figure 2-3 A). Carbonate veins are abundant in these dykes.

Of the three, only type-I dykes regularly host quartz veins and sulfides, whereas type-II dykes do not host quartz veins or sulfides (except rarely on their margins), and type-III dykes do not host quartz veins or sulfides.

2.3.2 Structure and Deformation

Five deformation events are observed based on overprinting relationships. The first, D_1, is defined by the Tuludimtu and Bedele shear zones, along which the Tulu Kapi syenite is found. These shear zones are thought to have been dilatational conduits that focused intrusion of the syenite magma (Kebede, 1999). D_2 is the earliest deformation event that effected the syenite. While its kinematics is not certain, D_2 resulted in vertical faults which are overprinted by D_3 deformation. D_3 reflects a compressional regime with reverse faulting, which then evolved to strike-slip for D_4. D_5 is interpreted as late extensional tectonics during orogenic collapse.

The earliest deformation in the syenite is vertical D_2 faulting. The faults are either intruded by type-I dykes or are surrounded by a bleached halo with occasional cataclasites and shearing. A portion of these early dykes strike north to northeast and are vertical, but generally their orientation varies from drill core measurements (Figure 2-4 A), but are consistently modelled to be northeast striking (Figure 2-1).

The most pervasive fabric in the study area is a northeast striking, vertical to steeply dipping S_3 foliation (Figure 2-4 B), which strikes parallel to the Tuludimtu and Bedele shear zones. The foliation is found in the south-eastern sheared margin of the Tulu Kapi syenite, Bedele shear zone, Kapi gabbro and the trachyte. Earlier foliations in the area may have been obliterated during D_3 deformation.

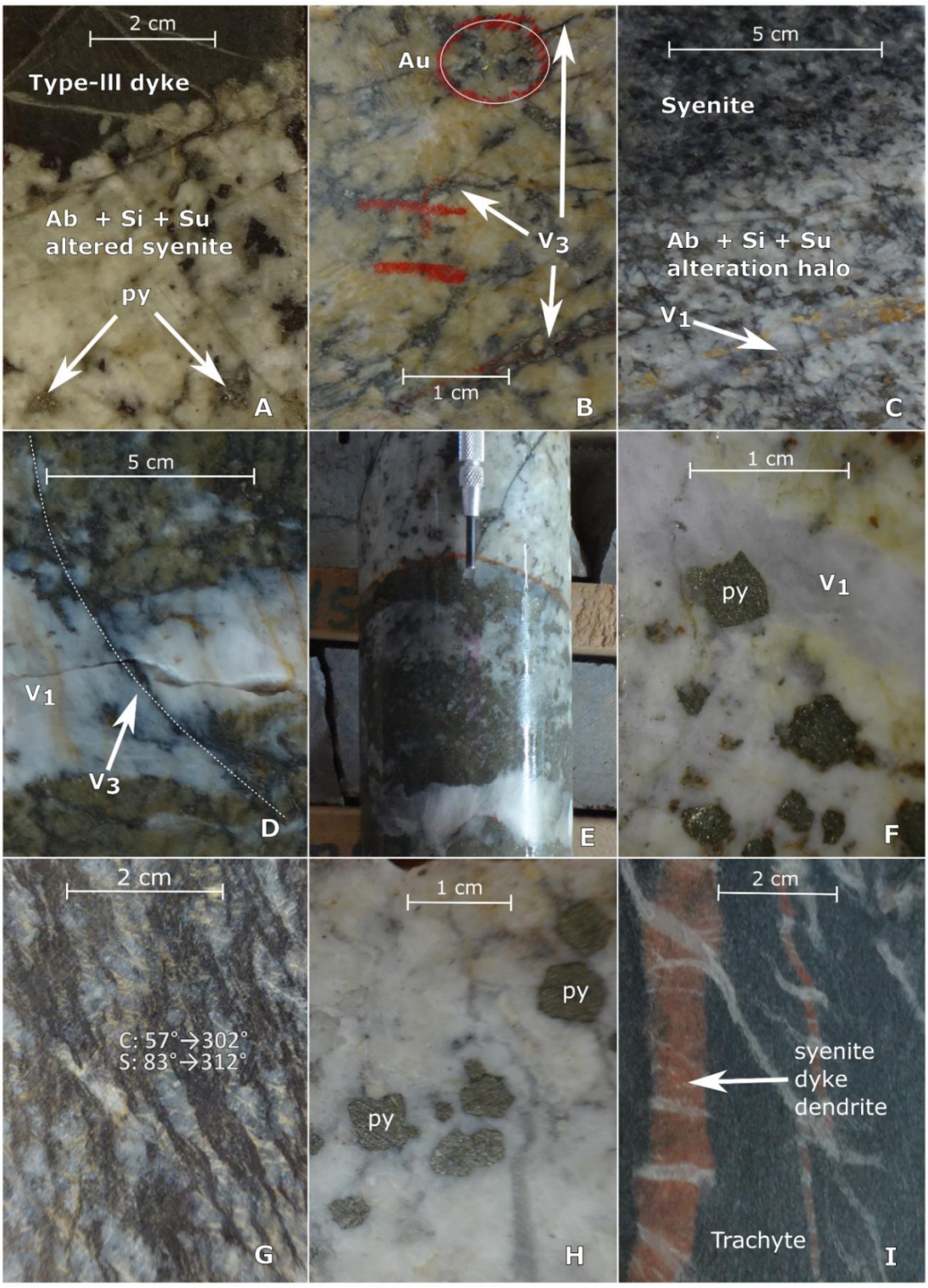
2 cm
Type-III dyke
Ab + Si + Su
altered syenite
py
A
Au
V3
1 cm
B
5 cm
Syenite
Ab + Si + Su
alteration halo
V1
C
5 cm
V1
V3
D
E
1 cm
py
V1
F
2 cm
C: 57°→302°
S: 83°→312°
G
1 cm
py
py
H
2 cm
syenite
dyke
dendrite
Trachyte
I

Figure 2-3: Veins, alteration and mineralization at Tulu Kapi. A: late type-III dyke in altered syenite; B: visible gold in fracture; C: gradational Ab + Si + Su alteration around V_1; D: V_3 overprinting V_1; E: polyphase quartz sulfide V_1; F: V_1 with euhedral pyrite overgrowing vein – wallrock contact; G: S-C fabric in the deep shoot; H: euhedral and hexagonal pyrite in albite altered syenite; I: syenite dyke dendrites in trachyte brittle deformation is preferentially in the dyke.

On foliation planes in the syenite, stretching lineations plunge steeply northeast (Figure 2-4 B). While shear plane development in the syenite pluton is rarely observed, when found it is broadly parallel to the Bedele shear zone (Figure 2-4 B; Figure 2-5 B). In the syenite adjacent to the Bedele shear zone, CS fabric indicates west-over-east reverse movement (Figure 2-3 G). Compressional tectonics with reverse faulting prevailed locally in Tulu Kapi during D_3.

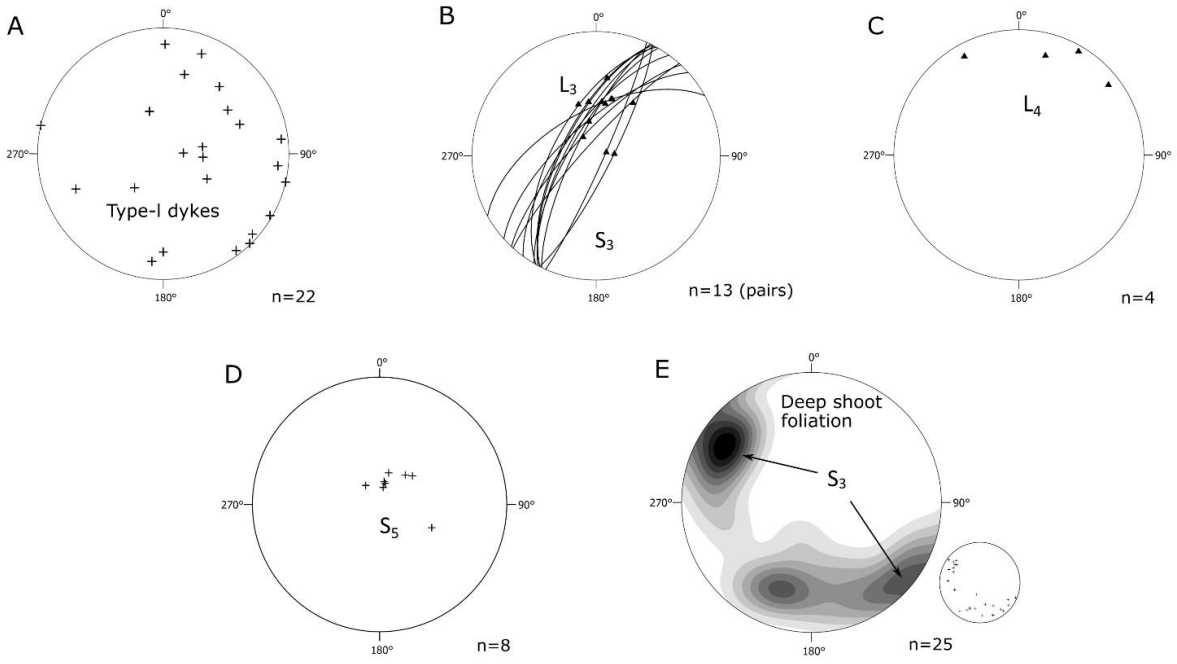

Figure 2-4: Orientations of structures at Tulu Kapi: Equal area, lower hemisphere projections were made using Stereo32™ software. A: poles to Type-I dykes (from oriented drill core); B: S_3 (great circles) and L_3 (triangles) pairs in the Bedele shear zone and Tulu Kapi deep shoot (from oriented drill core and outcrop); C: L_4 mineral stretching lineation (from oriented drill core);

D: S_5 poles in the Bedele shear zone (from oriented drill core); E: foliation poles in the deep shoot (from oriented drill core).

Sub-horizontal to shallow L_4 is observed on en-echelon vein surfaces, parallel to the strike of steep S_3 foliation (Figure 2-4 C). The shallow lineation together with its orientation indicates strike-slip movement for D_4. Previous workers in the WES have observed strike-slip movement post-dating thrusting (Braathen et al., 2001; Johnson et al., 2011; Fritz et al., 2013). Sinistral strike-slip faults are northwest striking in the WES as reported by Fritz et al. (2013), for example the Chochi Shear Zone, which offsets the Tuludimtu shear zone near Baruda (Figure 1-2), and the Surma Shear Zone in the southern WES (Figure 1-2).

Where the syenite's footwall contact with the volcanic units intersects the Bedele shear zone, a crenulation foliation overprints S_3. The foliation is gently south dipping. In the syenite, near the footwall contact with the volcanic units, sub-horizontally west or east plunging fold hinges are found. These structures are not compatible with strike-slip movement during D_4 and postdate D_3, and so belong to a later deformation event, D_5. D_5 structures are compatible with north-south directed sub-horizontal movement, which in the region have been recognized by Yihunie and Hailu (2007), who postulated that they were products of late orogenic collapse.

2.3.3 Major Structure: The Bedele shear zone

The Bedele shear zone is a D_1 structure which is thought to have played a localizing role during the intrusion of the Tulu Kapi syenite. The Bedele shear zone strikes northeast at Tulu Kapi following the edge of the syenite and gabbro intrusions. To the north-northeast of Tulu Kapi, it continues to join the cross-continental Tuludimtu shear zone (Figure 1-2 and Figure 2-1). Adjacent to Tulu Kapi, the Bedele shear zone is several hundred meters wide. Mylonitic textures are typical with occasional fragments of syenite and other country rock. From the three-dimensional modelling of drillholes, the Bedele shear zone contact with the syenite and trachyte unit dips 56° towards 313°.

2.4 Veining/Structure

Gold mineralization and its associated alteration are found in rocks containing quartz + sulfide ± carbonate veins (KEFI Minerals Plc., 2015). This veining is found on the east side of the elongated Tulu Kapi syenite pluton, the side in contact with the Bedele shear zone; veining diminishes with distance from the shear zone (Figure 2-1).

2.4.1 Veins

There are four dominant vein types at Tulu Kapi (Table 2-2-1). Three of them are found in the alteration zones associated with gold mineralization, and the fourth one along a litho-tectonic contact between the Tulu Kapi syenite and Bedele shear zone (Table 2-2-1).

Table 2-2-1: Veins in the altered lodes of Tulu Kapi.

Vein	Type	Infill (major)	Infill (minor)	Wallrock Texture
V_1	En-echelon	Quartz	Pyrite ± carbonate ± galena ± sphalerite ± arsenopyrite ± chalcopyrite	Massive or sheared
V_2	Fault/Fracture fill	Quartz	Pyrite ± pyrrhotite ± carbonate ±chlorite ± galena ± sphalerite ± chalcopyrite ± gold	Sheared, broken or massive
V_3	Narrow fracture	Pyrite ± pyrrhotite ± galena ± sphalerite	Carbonate ± chlorite ± quartz ± gold	Massive
V_4	Contact fill	Quartz	Pyrite ± galena ± sphalerite	Sheared

V_1 en-echelon arrays are planar, and mostly sub-horizontal to gently west dipping, and are oriented ~45° to the Bedele shear zone and other shears in the syenite (Figure 2-5 A and B; Figure 2-6 C and D). They are found in the Tulu Kapi syenite along the contact with the Bedele shear zone and throughout the syenite pluton within several hundred meters of the Bedele shear zone, including

inside type-I dykes (Figure 2-1). In drill core, rock adjacent to the en-echelon arrays is typically massive, but occasionally sheared. In outcrop, en-echelon arrays can be found bound by shears (Figure 2-6 C and F). Outcropping shears can be one of, discrete zones in the syenite (Figure 2-6 C and F), the contact between the Bedele shear zone and the syenite (Figure 2-6 E), or sheared type-II dykes (Figure 2-6 A). En-echelon veins are central to Ab + Si + Su altered lodes; mineralization-associated alteration gradationally diminishes with distance from the veins (Figure 2-3 C). The veins are continuous for decametres in outcrop. Their thicknesses vary from sub-centimetre to several centimetres. The veins are composed of quartz ± sulfide ± carbonate.

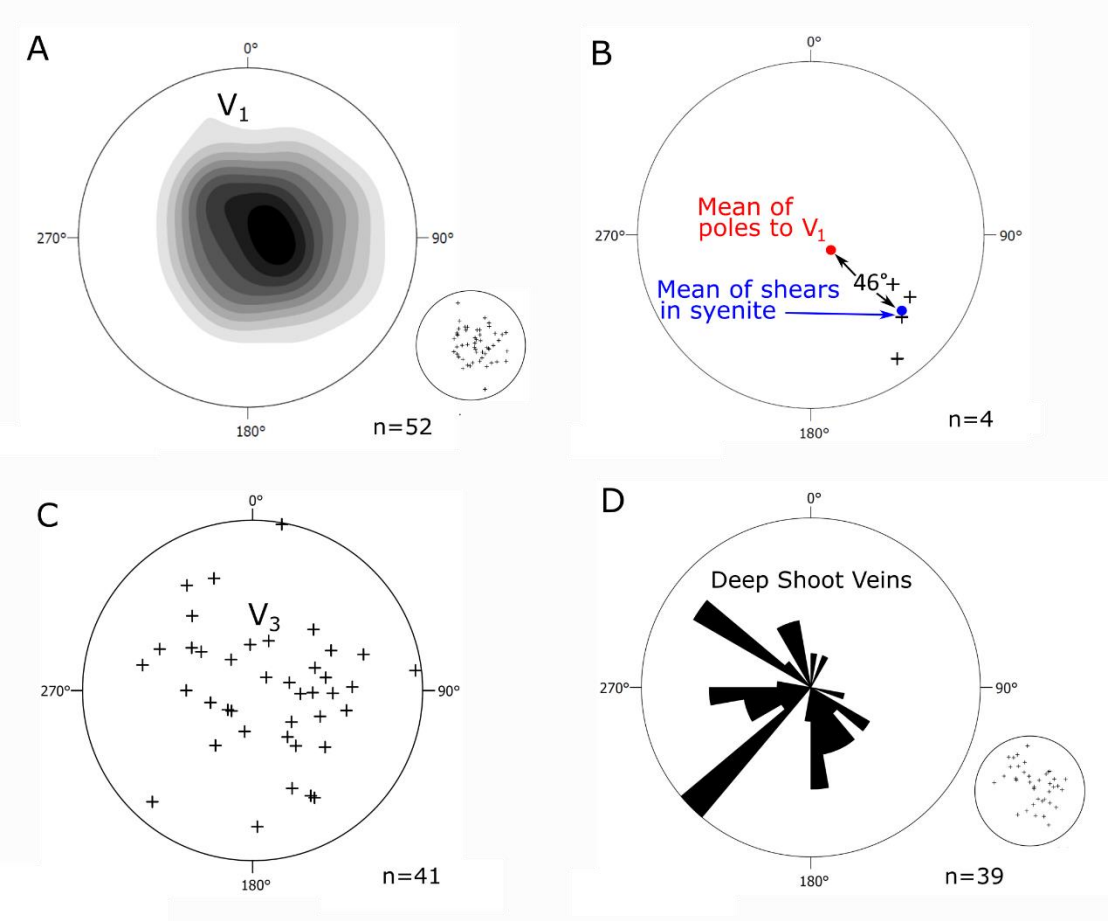

Figure 2-5: Orientations of veins at Tulu Kapi; equal area, lower hemisphere stereographic projections using Stereo32™ software. A: V_1 poles (from oriented drill core); B: D_3 shear planes

in the syenite and mean pole of V_1 in the syenite; means and angle calculated in Stereo32™ (from oriented drill core); C: V_3 poles (from oriented drill core); D: veins in the deep shoot as dip direction rose diagram and poles (inset) (from oriented drill core).

V_2 fault and fracture infill veins cross-cut en-echelon vein-bounding shears (Figure 2-6 C – pink line). They are moderately northwest dipping. Cataclasite and mylonite are occasionally found in the veins. V_2 veins are centimetres in thickness. They are composed of quartz + sulfides ± carbonate ± chlorite. V_2 in deep drillhole intersections are frequently brecciated. Breccia veins have matrices of quartz, carbonate, pyrite and pyrrhotite and clasts are wallrock, pyrite, sphalerite and galena.

V_3 veins are spatially associated with and cut across V_1 veins (Figure 2-3 D). V_3 veins are on average steeper than V_1 veins (Figure 2-5 C), are laterally continuous over centimetres to decimetres, are sub-millimetres to millimetres in width and are composed of sulfides ± carbonate ± quartz ± chlorite.

V_4 occupies a portion of the contact between the Tulu Kapi syenite and Bedele shear zone. Sheared wall-rock fragments can be found in the vein. At its maximum width, it is over one metre in true-thickness (Figure 2-6 B). The vein is comprised of quartz with polymetallic sulfides infilling fractures with occasional centimetre-scale euhedral sulfides.

2.5 Gold Mineralization and Alteration

2.5.1 Gold Mineralized Veins

In the syenite, V_1, V_2 and V_3, as well as the contact between the Tulu Kapi syenite and the Bedele shear zone (V_4) host gold. The Kapi gabbro is host to gold mineralized quartz veins not in en-echelon arrays, but in lone veins. Vein arrays are found in type-I dykes in the gabbro. Due to the paucity of outcrop and minimal drilling, only one quartz-sulfide vein containing visible gold in the gabbro was measured in oriented drill core; the vein is sub-horizontal (12°→040°). It is uncertain which generation the vein belongs to.

In quartz veins, gold is found along grain boundaries of pyrite or pyrrhotite (Figure 2-7 B), in quartz (Figure 2-7 A), filling fractures in pyrite (Figure 2-7 D), or as inclusions in pyrite (Figure 2-7 C). Visible gold is found in breccia veins (V_2) and V_3 fractures near the footwall of the syenite,

typically at depths below approximately 300 meters from surface in the deposit, in an area referred to as the deep shoot.

Throughout the deposit, gold lodes contain compositionally heterogeneous veins with zoned quartz, carbonate and sulfide minerals. They are here referred to as polyphase veins reflecting the multiple fluid phases they appear to have accommodated. These veins exhibit zoning of hydrothermal quartz, sulfides and carbonates. Polyphase veins exhibit early and late quartz and multiple sulfide phases (Figure 2-3 E); V_1, V_2 and V_4 are noted to exhibit polyphase character.

2.5.2 The Deep Shoot

The Tulu Kapi deep shoot, found at a depth of approximately 300 meters from surface and below, is in a highly deformed zone of the syenite adjacent to its footwall. It is found adjacent to the syenite's contact with the Bedele shear zone, Kapi gabbro and trachyte. It is bound by the southern dyke swarm to the south, but its northern limit has not been delineated through drilling. Concentration of gold in the shoot is more than twice that of shallower mineralization (Olssen and Cleghorn, 2015). The shoot features superimposed vein sets and dense fracture networks resulting in a vein stockwork. Veins dip towards four main directions, northwest, west, southwest and southeast (Figure 2-5 D). Veins are found to have formed parallel to the strike of foliation (but with substantially shallower dip) (Figure 2-4 E; Figure 2-5 D). S_3 foliation planes in the deep shoot are parallel with ones found in the outcropping Bedele shear zone. The northeast dipping foliation in the shoot has not been found elsewhere in the study area, this foliation is parallel to the syenite's contact with the trachyte. No overprinting relationship was observed between the foliation sets.

2.5.3 Alteration

Five types of alteration are commonly found in Tulu Kapi are: magnetite, biotite, albite/silica/sulfide (Ab + Si + Su), carbonate and chlorite. Magnetite alteration is found throughout the region, and locally in the syenite pluton, the gabbro and in the early porphyritic dykes except for: (1) In Ab + Si + Su altered syenite lodes, and (2) in type-II and III dykes and their wallrock and adjacent to faults such as, the Tulu Kapi syenite contact with the Bedele shear zone.

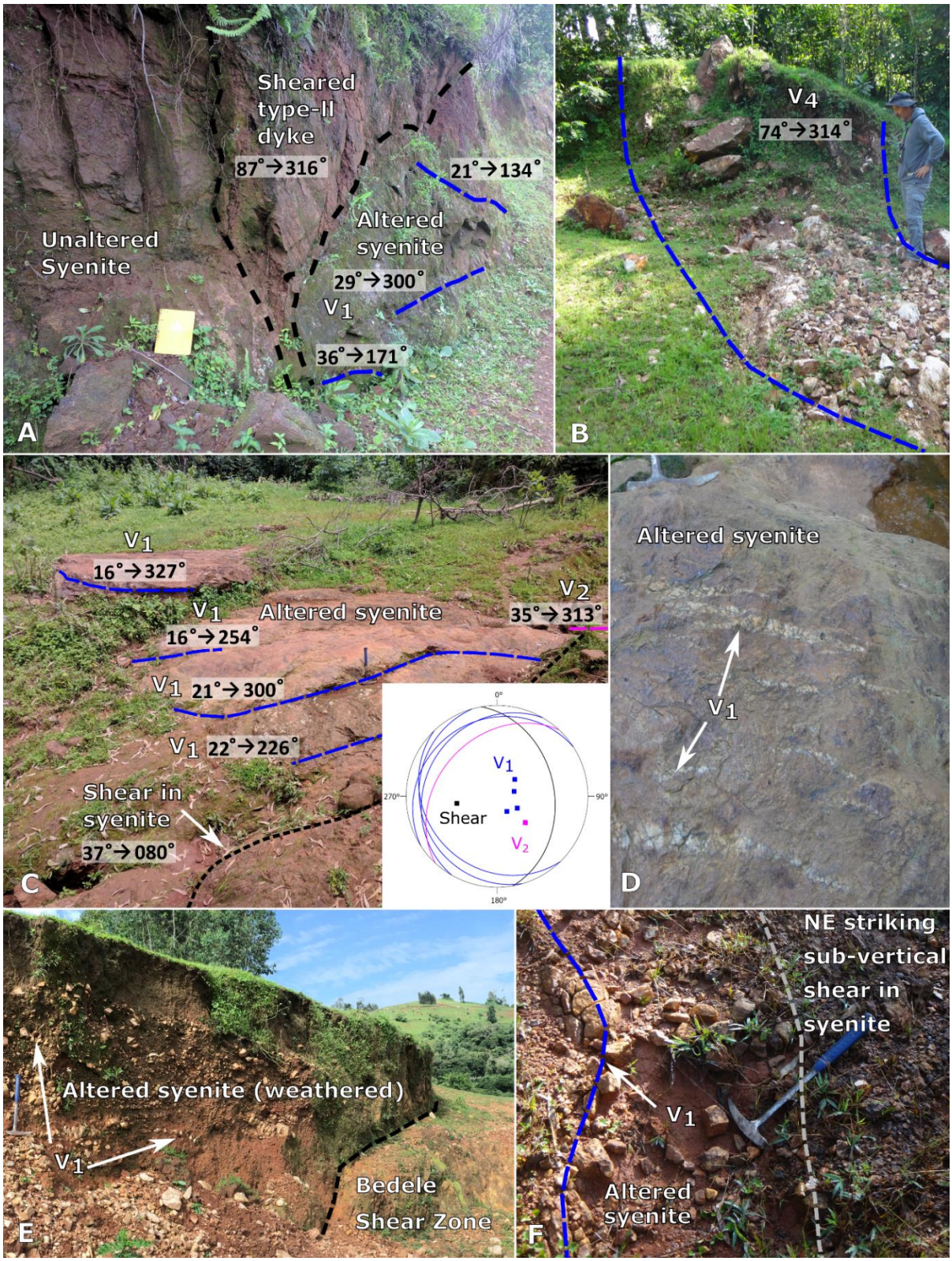
Sheared type-II dyke
87°→316°
21°→134°
Altered syenite
29°→300°
V1
36°→171°
Unaltered Syenite
A
V4
74°→314°
B
V1
16°→327°
V1
16°→254°
Altered syenite
V2
35°→313°
V1 21°→300°
V1 22°→226°
Shear in syenite
37°→080°
C
0°
90°
180°
270°
V1
Shear
V2
Altered syenite
V1
D
Altered syenite (weathered)
V1
Bedele Shear Zone
E
NE striking sub-vertical shear in syenite
V1
Altered syenite
F

Figure 2-6: Veining and contacts in outcrop. A: V1 (blue) terminating against a sheared type-II dyke (black); on the far-side of the dyke the syenite is unaltered. B: V4 in outcrop. C: V1 (blue) terminating against a shear zone (black) and V2 cross-cutting shear zone. Stereoplot: V1 (blue) 45 to 58° to shear zone (black), V2 (pink). D: V1 between sheared dyke and Bedele shear zone contact. E: Tulu Kapi syenite and Bedele shear zone contact (black) with V1 in syenite. F: northeast striking shear in the syenite with adjacent northwest dipping V1.

Biotite alteration of the syenite is proximal to the Bedele shear zone (KEFI Minerals Plc., 2015). The biotite alteration gives the syenite a distinctive dark colour. Biotite diminishes with the intensity of Ab + Si + Su alteration.

Albite, silica and sulfides (pyrite and pyrrhotite) occur together in leucocratic alteration lodes. It has not been determined whether these three alteration products are coeval or not. They are grouped together due to their common occurrence (Figure 2-3 A, F and H). In the gold deposit, Ab + Si + Su alteration is found in the syenite and type-I dykes exclusively, where K-feldspar is altered to albite. In thin section, albite rims can be found on K-feldspar (Figure 2-2 B; Figure 2-7 F). In outcrop and drill core, albite alteration is adjacent to V_1 and V_2 and diminishes gradationally away from them (Figure 2-3 C). Albite alteration zones are accompanied by disseminated sulfide minerals in the wall-rock; most commonly pyrite and/or pyrrhotite. Pyrrhotite abundance in the alteration zones increases with depth in the syenite. There is a strong association between elevated gold mineralization and Ab + Si + Su alteration (KEFI Minerals Plc., 2015).

Calcite is found as sub-mm to cm scale veins in the syenite and all dyke types. In the deep shoot, calcite is found filling voids in the syenite adjacent to pyrrhotite. Carbonates in the Tulu Kapi syenite are most widely distributed in the region immediately adjacent to the Bedele shear zone but can be found throughout the syenite and gabbro including all contained dykes.

Chlorite is found throughout the Tulu Kapi area and not restricted to alteration zones associated with gold mineralization. The Tulu Kapi syenite and Kapi gabbro both contain abundant chlorite.

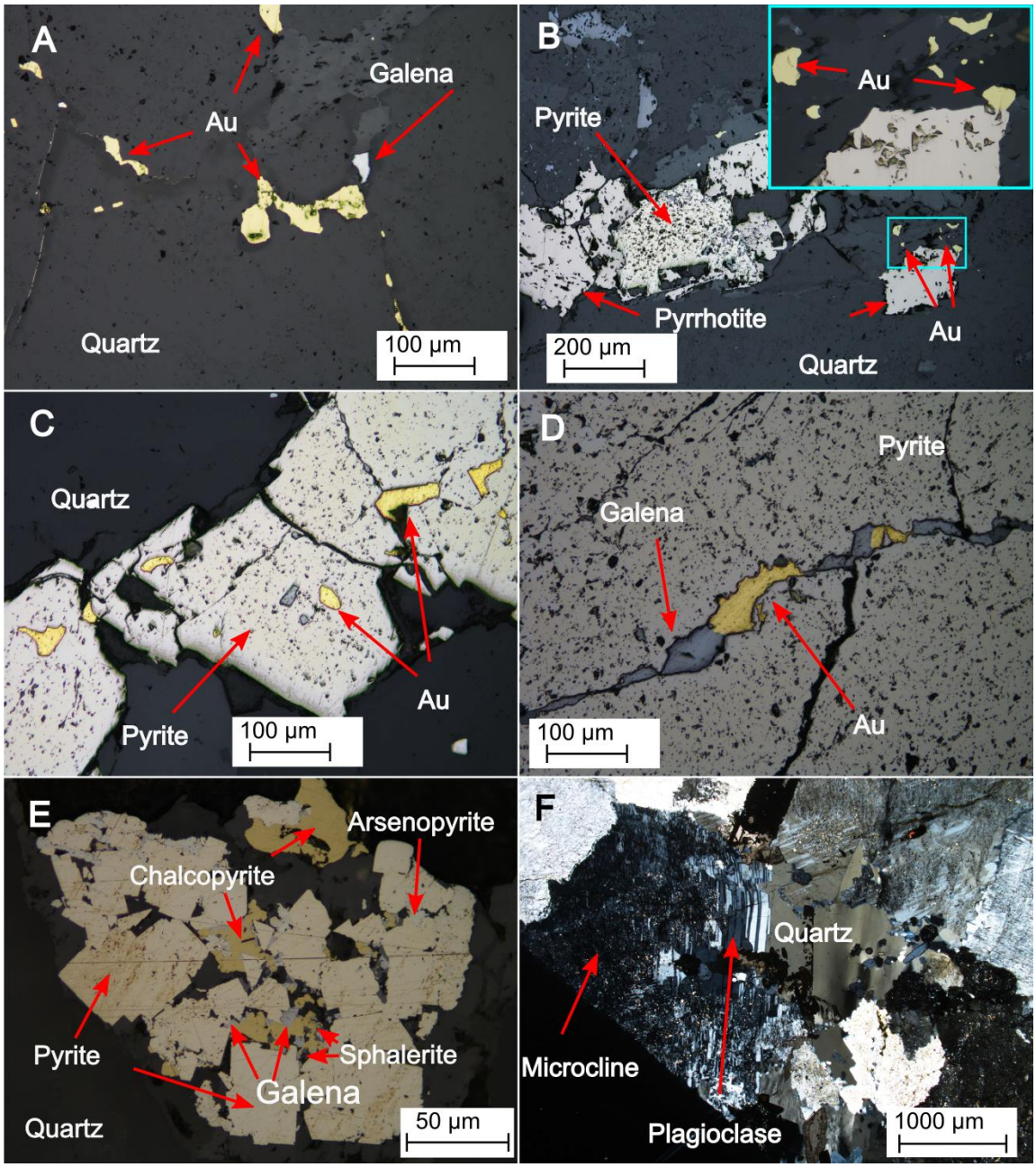

Figure 2-7: Ore mineral petrology in plane polarized reflected light from A to E, and F is cross-polarized transmitted light. A: gold in a quartz vein; B: pyrrhotite overgrowing pyrite with later gold; C: gold in pyrite; D: gold and galena infilling a fracture in pyrite; E: early pyrite with later arsenopyrite, galena and sphalerite, and late chalcopyrite; F: Microcline altered to orthoclase adjacent to quartz.

2.5.4 Sulfide minerals

Sulfide minerals are found in the syenite, dykes, gabbro, the trachyte and the Bedele shear zone. The most common sulfides are pyrite and then pyrrhotite. Pyrite is found in all units whereas pyrrhotite, galena, sphalerite and chalcopyrite are mostly restricted to the syenite, gabbro and type-I dykes.

Disseminated pyrite is abundant in Ab + Si + Su alteration lodes and is found in all vein types. In Ab + Si + Su alteration zones where pyrite is the only sulfide mineral, it is typically cubic, euhedral and forms hexagonal polycrystalline masses (Figure 2-3 F and H). In the syenite, pyrite-bearing veins are sometimes sheared with pyrite clearly predating the foliation and ~1 mm pyrite overprint shear foliation.

In Tulu Kapi, at depths of approximately 300 meters and below, pyrrhotite occurs in veins and is the dominant disseminated sulfide in the wall-rock. Disseminated pyrrhotite frequently occurs adjacent to carbonates and can be accompanied by pyrite, galena and sphalerite. In shallow portions of Tulu Kapi (up to ~150 meters deep), pyrrhotite is disseminated or in veins proximal to the southern dyke-swarm only.

The proportion of base metal sulfides in wallrock and veins generally increases with depth, but these minerals are also found in V_4, which outcrops. In drill core, sphalerite and galena are disseminated in the wallrock, as well as in all vein types. Chalcopyrite overgrows pyrite, pyrrhotite, galena and sphalerite (Figure 2-7 E); but it can also be found encapsulated in pyrite and pyrrhotite. Arsenopyrite is rare, but is found in the northern and western portions of the gold deposit as well in and around the deep shoot.

Gold is found in quartz and breccia veins filling fractures and is commonly adjacent to pyrite and pyrrhotite. Gold also fills fractures in pyrite and occurs as isolated grains as inclusions in pyrite. Occasionally, galena fills the same fractures in pyrite as gold (Figure 2-7 D).

Fe-oxides are found in the syenite but not in Ab + Si + Su altered lodes. In outcrop, drill core and thin section, magnetite is abundant. Ilmenite is commonly spatially association with magnetite.

2.6 U-Pb Geochronology

2.6.1 Methods

Nine samples were selected for U–Pb geochronology. However, seven of these samples yielded scattered zircon U/Pb analyses that did not conform to single or multiple statistically distinct populations. The results for these seven samples are presented in the Appendix. The detailed results from the remaining two samples (Sample D_03 from the Tulu Kapi syenite pluton and D_06 from the Kapi gabbro) are reported below. All samples were crushed to 2 mm using a jaw crusher at Tulu Kapi, Ethiopia. Crushed samples were sent to Northwestern University in Xian, China for standard magnetic and heavy liquid separation. Zircons were mounted in epoxy disks, polished, and imaged with backscatter and cathodoluminescence at Northwestern University in Xian, China.

U–Pb zircon geochronology was conducted at the Metal Isotope and Geochemistry Laboratory at the University of Waterloo using an Analyte G2 193nm Excimer laser coupled to an Agilent 8800 triple quadrupole ICP-MS. The primary reference material was 91500 (1065 Ma; Wiedenbeck et al., 1995). Plesovice (337 Ma; Sláma et al., 2008) and R33 (419 Ma; Black et al., 2004) were used as secondary reference materials. The laser was operated with a sample surface energy of 4 J/cm^2 (measured at the sample surface), a spot size of 25μm, and a repetition rate of 5 Hz. The aerosol was carried to the torch with ~0.5 L/min of He and ~1.5 L/min of Ar makeup gas was added between the ablation cell and the torch. The following masses were measured with dwell times in brackets: ^{91}Zr (0.01s), ^{202}Hg (0.01s), ^{204}Pb (0.05s), ^{206}Pb (0.035s), ^{207}Pb (0.075s), ^{208}Pb (0.01s), ^{232}Th (0.01s) and ^{238}U (0.015s). Samples and standards were ablated with three cleaning pulses, followed by the collection of a 20s background and 30 s of ablation. Standard–sample bracketing was used and the primary standard was analyzed every 5–6 analyses. Data were reduced using Iolite v3.6 and the U-Pb_Geochron4 data reduction scheme (Paton et al., 2011). Secondary standard Plesovice yielded an age of 337.1 +/- 1.3 Ma (2SD, n=84/87), which is within analytical uncertainty of the reference value. R33 yielded an age of 413.1+/- 3.9 (2SD, n=20/22), which is slightly younger than the accepted TIMS age.

2.6.2 Results

D_03 and D_06 yielded a sufficient number of well zoned, unfractured zircons of suitable size for analysis (Figure 2-8). Zircons from sample D_03 (Tulu Kapi syenite) are 50–200 μm in length with

flat to oscillatory zoning in cathodoluminescence and have aspect ratios of 2:1. The results of 53 analyses are shown in Figure 2-9. Twenty-six analyses plot off concordia towards the composition of common Pb and are excluded from the weighted mean age calculation. One analysis plots off concordia at a younger age; the geological significance of this is unclear but this analysis may reflect radiogenic lead loss. Twenty-six analyses that overlap concordia yield a weighted $^{238}U/^{206}Pb$ age of 738.3 ± 2.6 Ma (2s, MSWD= 1.12) (Figure 2-9). This is interpreted as the crystallization age of the syenite.

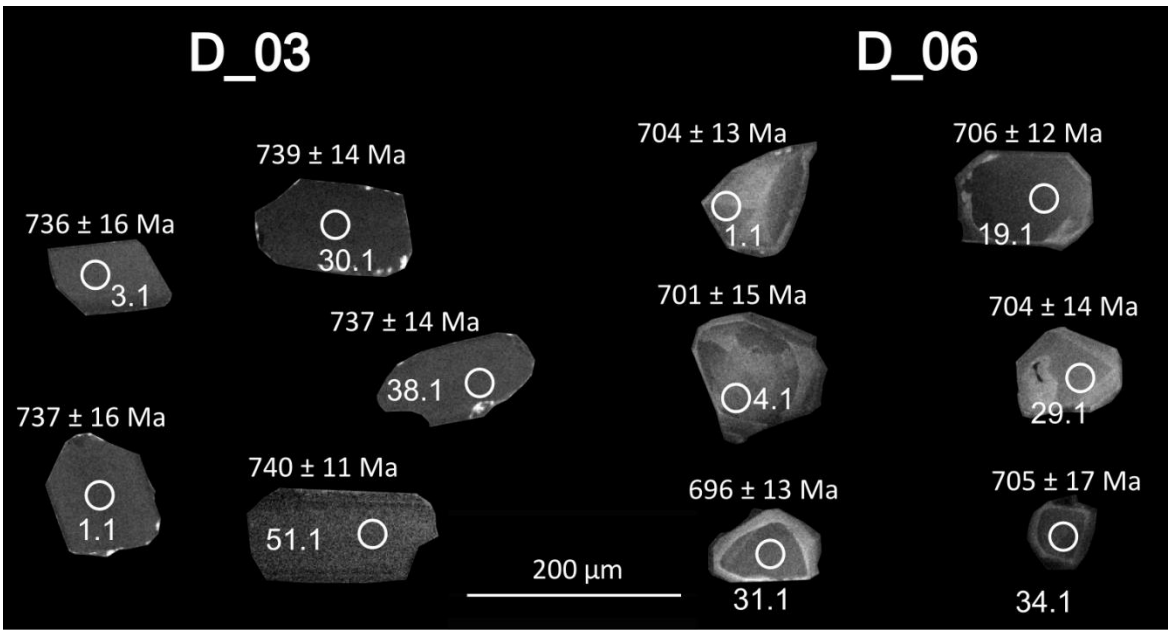

Figure 2-8: Cathodoluminescence images of zircons analysed for U–Pb zircon geochronology of the Tulu Kapi syenite, D_03, and Kapi gabbro D_06. Circles are 25 µm diameter spots and ages are reported with their two standard deviation uncertainties.

Zircons from sample D_06 (Kapi gabbro) are 50–150 µm in length with oscillatory zoning in cathodoluminescence and have aspect ratios of 1:1 to 1.5:1. The results of 47 analyses are shown in Figure 2-9. Twelve analyses plot off concordia towards the composition of common Pb and are excluded from the weighted mean age calculation. One analysis plots off concordia at a younger age; the geological significance of this is unclear but this analysis may reflect substantial radiogenic lead

loss. Thirty-five analyses that overlap Concordia yield a weighted $^{238}U/^{206}Pb$ age of 699.5 ± 2.7 Ma (2s, MSWD= 1.3) (Figure 2-9). This is interpreted as the crystallization age of the gabbro.

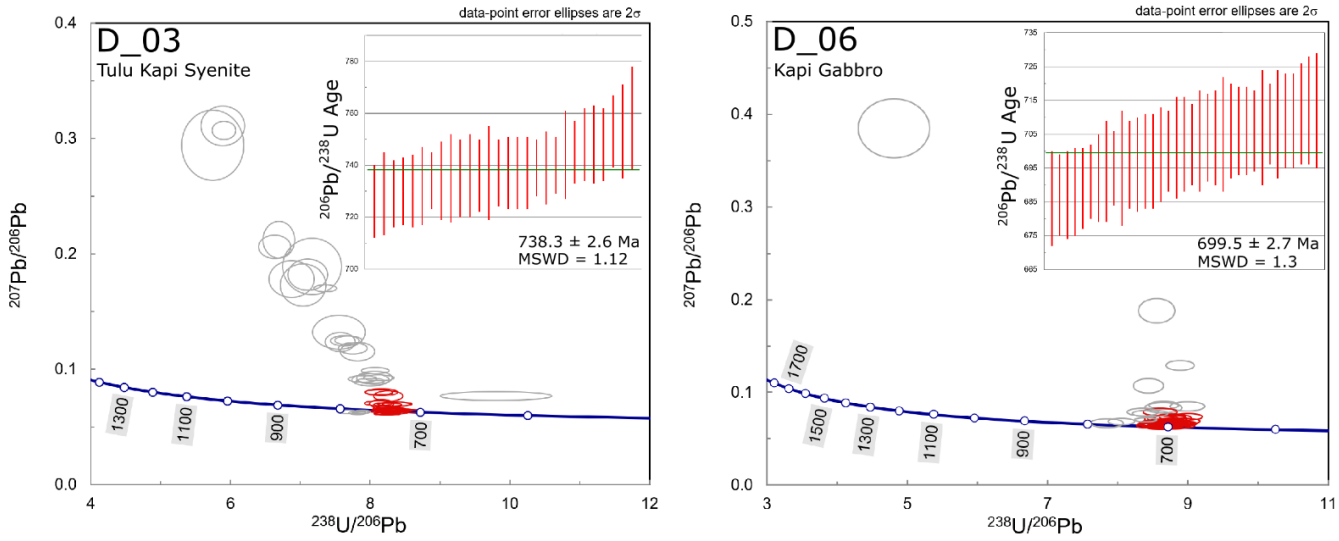

Figure 2-9: Tera–Wasserburg concordia diagrams for D_03 and D_06. The inset weighted average plot shows the data used to calculate 206Pb/238U weighted mean ages. Red ellipses were used in weighted mean age calculations.

2.7 Discussion

2.7.1 Controls on Mineralization

2.7.1.1 Regional Controls

From a regional perspective, the Tuludimtu shear zone had the greatest influence on the location of the syenite, its deformation and mineralization. Kebede et al. (1999) suggested that the magma that formed the Tulu Kapi syenite ascended through the crust along the Tuludimtu shear zone. Following syenite crystallization, it underwent brittle deformation during D_3 and D_4 which are regional deformation events in the WES. The deformed syenite was probably more permeable and probably focused the ascent of fluids that were transiting the Tuludimtu and Bedele shear zones during deformation.

2.7.1.2 Structural control of veins

Historically, mineralized lodes were modelled for the Tulu Kapi gold deposit. The modelling was driven by vein measurements as well as alteration logs and constrained within a dense drill grid (KEFI Minerals Plc., 2015). The modelled lodes form west-northwest dipping, stacked en-echelon arrays (Figure 2-10) (KEFI Minerals Plc., 2015).

V_1 in outcrop and drill core exhibit a 45° angular relation to adjacent shears (Figure 2-5 A and B and Figure 2-6 C). The average of V_1 is used from drill core measurements (Figure 2-5 A and B), since drill core data is not as accurate as outcrop data due to the small view field of the vein being measured. Veins in active shear zones should form at 45° to the shear zone (Ramsay and Graham, 1970). Pre-existing veins, with shear zones forming after the veins, will not show this special angular relation (Ramsay, 1967). The orientation of outcropping en-echelon veins to shear zones and shears in the syenite in Tulu Kapi implies that they formed during D_3 reverse movement along the Bedele shear zone.

While hundreds of portions of vein arrays were studied in outcrop and diamond drill core, it was rare to observe shear zones in the syenite wallrock of the vein arrays, particularly in drill core. Shears were more readily observed in outcrop, perhaps due to the shears becoming more readily identifiable once weathered. Robert and Poulsen (2001) advocate that vein systems can define shear zones where the shears themselves are poorly developed or difficult to map. Since the veins in the en-echelon arrays are not sigmoidal, there was likely no significant deformation along the shears in the syenite after the en-echelon arranged fractures formed. En-echelon veins are expected to form during the initial stages of shear zone development in competent units (e.g. Hodgson, 1989), like in the syenite at Tulu Kapi. The lack of continuous deformation may have contributed to the poor development of shears in the syenite. Shear zones would be required for formation of the staked en-echelon vein arrays. Historically, the en-echelon lode stacks in Tulu Kapi were modelled continuously on the 100 meter, or deposit scale, suggesting that the shears which they are subordinate to should also be continuous on that same scale.

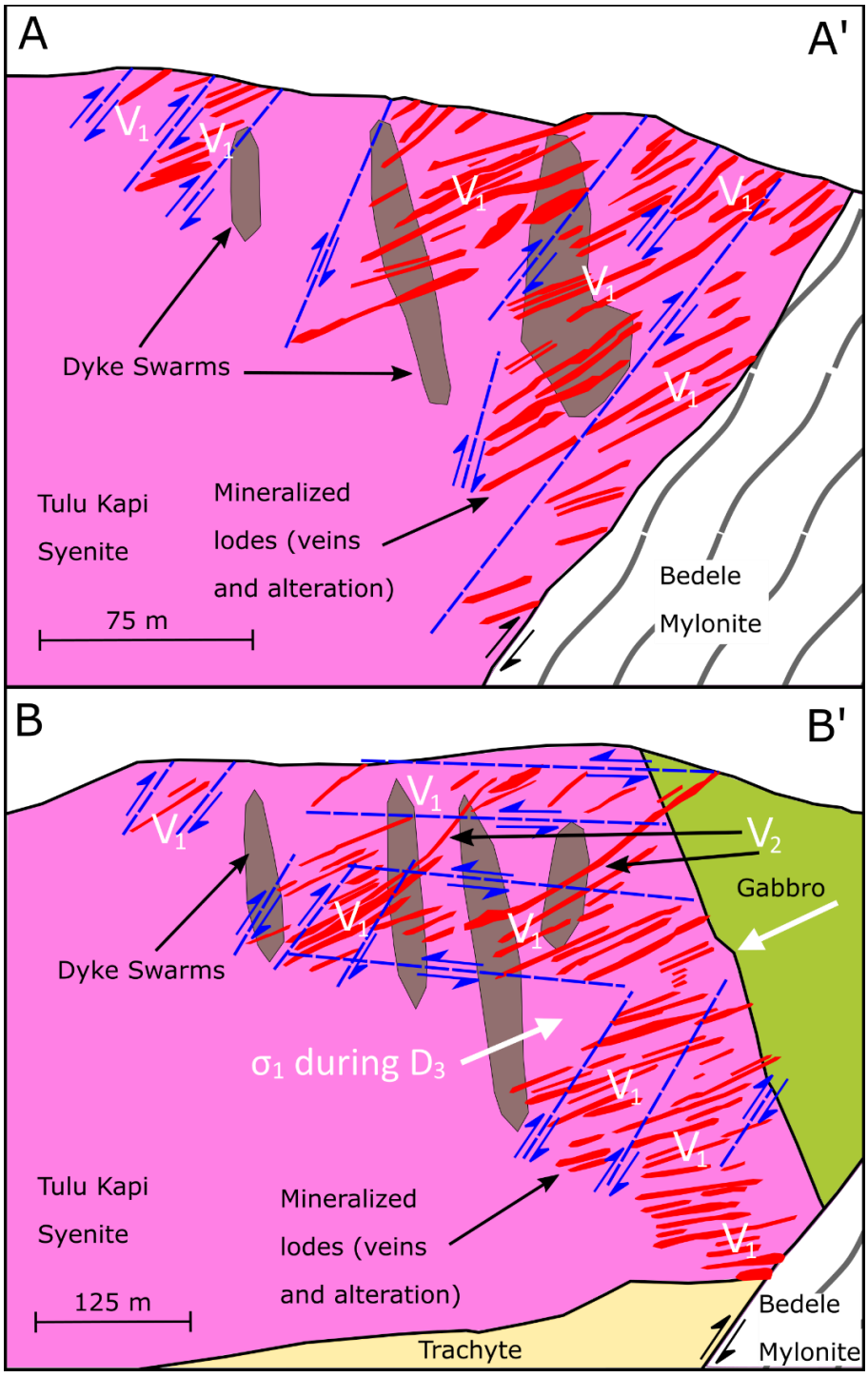

Figure 2-10: Veins and conjugate shears in cross-sections. Cross section locations as in Figure 2-1.

The vein-controlling shears in the syenite can be interpreted using the historical Tulu Kapi lode model and the Ramsay and Graham (1970) model for shear controlled en-echelon vein formation (Figure 2-10). The resulting interpretation concludes that the Tulu Kapi's modelled lodes and V_1 arrays are coincidental and their formation is consistent with reverse shearing on the Bedele shear zone.

In southern Tulu Kapi (Figure 2-10 A), the majority of interpreted shears are parallel to the Bedele shear zone. This orientation matches measurements taken of discrete shears in the syenite (Figure 2-5 B). In northern Tulu Kapi (Figure 2-10 B), a conjugate set of shears is interpreted to dominate locally, however, the Bedele shear zone-parallel shears still seem to dominate at depth, proximal to the syenite's contact with the Bedele shear zone. A sub-vertical, Bedele shear zone-strike parallel, shear is the only one found outcropping in northern Tulu Kapi (Figure 2-6 F).

The geometry of the interpreted shear system can be summarized by combining outcrop and drill core observations with interpretations: The orientations of shear zones that control the en-echelon vein arrays in Tulu Kapi are parallel to the contact between the Tulu Kapi syenite and Bedele shear zone and a conjugate set of shears. The orientation of the en-echelon veins does not vary greatly with the orientation of the controlling shear zone (Figure 2-10), suggesting that they are tension veins and not shear veins (Beach, 1975).

V_1 vein arrays and their controlling shears in the syenite probably formed at the same time; their orientation should indicate principle stress direction during the time of their formation. Sub-horizontal to gently west dipping V_1 (Figure 2-5 A) along with their steeply northwest dipping shears (Figure 2-5 B) and the Bedele shear zone, with its reverse sense of movement during D_3, all indicated a broadly NW directed principle stress axis at the time of their formation, D_3 (Figure 2-10 B). The orientation of the local minimum principle stress direction, near vertical during compression, would have been favourable for the dilation of shallowly to moderately dipping V_1 and V_2; which are the most dilated today. Fractures likely dilated during episodic fluid pumping events during D_3 with the Tuludimtu shear zone acting as the fault valve (e.g. Cox et al., 1986; Sibson et al., 1988).

V_2 cross-cuts a V_1 controlling shear in outcrop suggesting that V_2 is either part of the same deformation event as the shear, D_3, or later. V_2 can be observed in Figure 2-10 B to extend between

linear en-echelon arrays (whose central veins are V_1). V_2's orientation is conformable with the shears interpreted for the formation of V_1 and is thus likely to have formed during D_3.

V_3 sulfide veins are regularly found cross-cutting V_1 (Figure 2-3 D). V_3 veins formed after D_3 veins (V_1 and V_2) and their formation is thought to be coeval with mineralization, which is supported by the visible gold observed in them (Figure 2-3 B). Since there was deformation following D_3, D_3 veins had an opportunity to deform. The deformation could have been brittle and could be the reason why the deposit contains compositionally heterogeneous veins with zoned quartz, carbonate and sulfide minerals D_3 veins are found throughout the deposit.

The lack of steep veins and fractures in the syenite post-dating D_3 veining adjacent to the walls of the Bedele shear zone attest to the lack of significant movement along the Bedele shear zone during the strike-slip D_4 event. This lack of movement is likely due to the near-perpendicular angle which the Tuludimtu shear zone made with the west directed principle stress direction which was maintained during the protracted continental collision driving D_3 and D_4 (Braathen et al., 2001; Allen and Tadesse, 2004; Johnson et al., 2004; Fritz et al., 2013). Steep V_3 fractures are found adjacent to V_1. So, V_1 deformed during D_4. This deformation of V_1 during D_4 may have allowed gold-bearing fluids to permeate and precipitate gold.

The age of V_4, the vein along the contact of the syenite and Bedele shear zone is uncertain, but it may be coeval with V_1, however, it was likely continuously reworked due to its location.

2.7.1.1 Rheology

The Tulu Kapi syenite underwent brittle deformation, while the neighbouring rocks of the Bedele and Guji shear zones, which are thought to be mostly volcanic or sedimentary, underwent ductile deformation. Fractures preferentially found in syenite dendrites as opposed to the trachyte supports the syenite preferential fracturing (Figure 2-3 I).

2.7.1.2 Deep Shoot

The deep shoot is found on the footwall of the syenite, coincidental with a three-way tectonic intersection between the syenite, Bedele shear zone, trachyte and gabbro units. Differential movement at the three-way intersection was likely more common than along individual shear zones in the syenite and at contacts between the syenite and adjacent lithologies. Rocks in the deep shoot had a higher

likelihood of deforming than in other areas of the syenite due to being exposed to more differential movement between the four lithological units, thus, it now hosts denser fracture patterns. Foliation and fracture measurements suggest that there was shearing and related fracturing in multiple directions (Figure 2-4 E; Figure 2-5 D), as would be expected at such a complex junction. The network of fractures form a stockwork shoot. The deep shoot's dense fracturing and ideal location adjacent to the Bedele shear zone allowed it to be more amenable to fluid infiltration than other rocks in the deposit resulting in being endowed with higher gold grades.

2.7.1.3 Absolute timing of gold mineralization

The $^{206}Pb/^{238}U$ dates for the Tulu Kapi syenite and the Kapi gabbro, both of which host gold mineralization, are 738.3±2.6 Ma and 699.5±2.7 Ma, respectively. The post-tectonic Genji granite, with a $^{206}Pb/^{238}U$ age of 584±10 Ma (Blades et al., 2015), sits along the Tuludimtu shear zone to the south of the Tulu Kapi syenite. The Tuludimtu shear zone, a D_1 structure which the Bedele shear zone is a splay off of, would have to have been active during mineralization of the syenite in order to channel gold-bearing fluids, so the post-tectonic Genji granite temporally constrains gold mineralization. Gold mineralization is constrained between the crystallization ages of the Kapi gabbro and Genji granite, 699.5±2.7 Ma to 584±10 Ma respectively.

Gold mineralization in greenstone belts is typically syn-metamorphic. The presence of hexagonal euhedral habits of pyrite, but not in alteration zones containing polymetallic sulfides, suggest that the sufides in the alteration zone are pre or syn-peak-metamorphic (Craig and Vokes, 1993). Hence, the alteration zones are most likely to be either earlier than or coeval with gold mineralization. Metamorphism is documented between 635 and 580 Ma in the WES (Ayalew et al., 1990). This age for metamorphism sits within the age constraints provided by the Tulu Kapi and Genji intrusions that broadly bracket the timing of gold mineralization.

2.7.2 Regional Implications

2.7.2.1 Gold and tectonics

The age of the Tulu Kapi syenite (738.3 ± 2.6 Ma) represents a time in the Tuludimtu belt when arc formation is thought to have occurred in the ANS (Johnson et al., 2011). Fluid generated during metamorphism during or after orogenesis in the WES may have scavenged and transported gold prior

to transport through the crust via structurally-controlled faults and shear zones. A common element of intracratonic gold districts is their proximate location to transcratonic fault and shear zones which form as a result of continental collision, amalgamation and cratonization. The north-south trending Tuludimtu shear zone was an ideal conduit in the WES similar to the Larder Lake – Cadillac Fault Zone in the Superior Craton and Boulder-Lefroy Shear Zone in the Yilgarn Craton (Groves et al., 2000; Poulsen and Robert, 2000; Goldfarb et al., 2005).

2.7.2.2 Genetic model of Tulu Kapi

Based on microstructures, gold is either later than or coeval with Ab + Si + Su alteration, and postdates peak metamorphism (Figure 2-11). The mineral which could genetically be associated with gold is galena, which is found alongside gold filling fractures (Figure 2-7 D). Quartz, pyrite, pyrrhotite and galena are spatially associated with gold (Figure 2-7 A, B, C and D).

The Tulu Kapi syenite records multiple deformation events. D_3 to D_4 deformation fractured the syenite resulting in a more permeable unit where syn to post-D_4 auriferous fluids were channelled, resulting in structurally controlled gold mineralization in the syenite. The widest spread brittle structures in the deposit are D_3 conjugate shear-controlled linear en-echelon vein arrays, V_1, and shear adjoining faults, V_2, which were reopened and reactivated during D_4 allowing gold mineralization to be widely distributed through the syenite.

2.7.2.3 Absolute timing

The Tulu Kapi syenite (738.3 ± 2.6 Ma) hosts substantially more gold mineralization than the adjacent gabbro (699.5±2.7 Ma). The two intrusions are rheologically similar to one another as they are both crystalline intrusive rocks, yet the syenite hosts substantially more brittle structures, which is a likely reason for its superior endowment with gold. The earlier intrusion of the syenite likely exposed it to more opportunity for deformation than the gabbro; this probably made the syenite more permeable for auriferous fluids. With this line of reasoning, intrusions along the Tuludimtu shear zone which are as old as the Tulu Kapi syenite or older are to be more likely hosts to gold deposits than younger intrusions. However, the rheology of the intrusions is likely the primary control on their gold mineralization potential.

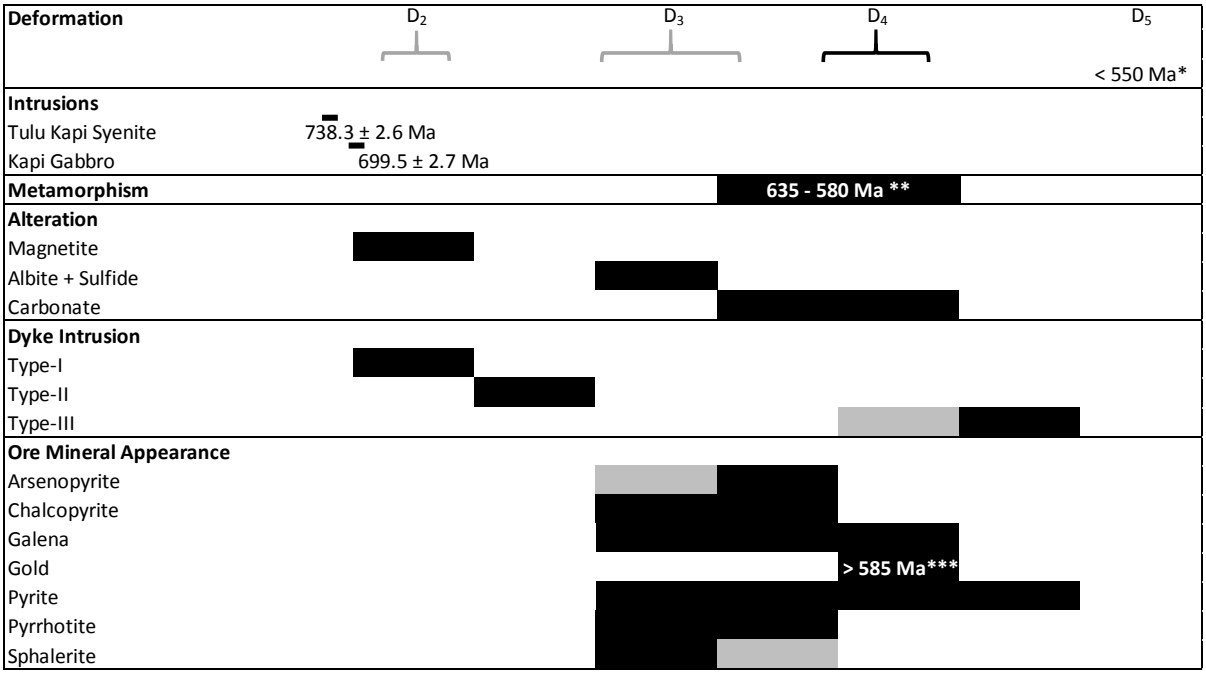

** Yihune and Hailu, 2007; ** Ayalew and Peccerillo, 1998; *** Blades et al., 2015*

Figure 2-11: Schematic representation of the sequence of events observed at Tulu Kapi. Black bars indicate higher confidence and grey bars indicate lower confidence.

2.7.2.4 Regional gold implications

Orogenic gold deposits commonly occur in belts and not in isolation. The presence of the epigenetic Tulu Kapi gold deposit is an indication of opportunity for gold exploration in the Kemashi domain along Tuludimtu shear zone.

Gold-bearing structures are found in the brittle Tulu Kapi syenite, but have not been found in adjacent ductile lithologies (Figure 2-3 I). The Tulu Kapi deposit can act as a model for targeted mineral reconnaissance and exploration in the Tuludimtu belt. The edges of pre-tectonic intrusions make primary targets, particularly where they are in contact with the Tuludimtu shear zone and its subordinate shears like the Bedele shear zone.

The apparent temporal association between galena and gold at Tulu Kapi is echoed by galena being the most abundant sulfide that is contemporaneous with gold mineralization at the Lega Dembi gold mine (Ghebreab et al., 1992) in the Southern Ethiopian Shield (Figure 1-1). Along with quartz and

pyrite, galena may be considered as a gold exploration vector along the Tuludimtu shear zone and possibly across the entire southern ANS.

Lithological contacts may have experienced differential movement which could have initiated veining, such as is the case with the Tulu Kapi syenite and Bedele shear zone contact. Alternatively, the contacts themselves could be mineralized if they were sheared, and, they may be particularly well endowed if dilatational structures, pull-apart structures, formed as is the likely case for V_4.

2.8 Sources of fluids

There are two commonly evoked sources of fluids in greenstone-hosted orogenic gold deposits, metamorphic and magmatic (Phillips and Powell, 2010; Goldfarb and Groves, 2015). The association of minor galena with gold is suggestive of an igneous-derived fluid (Goldfarb and Groves, 2015). However, the paucity of sulfides (other than pyrite and pyrrhotite) is more consistent with a metamorphic-derived fluid (Groves et al., 2003). The only know syn-kinematic magmatism along the Tuludimtu shear zone which postdates the Kapi gabbro is the Dogi Granite 50 km to the north of Tulu Kapi with a U-Pb titanite age of 651 ± 5 Ma (Grenne et al., 2003) (Figure 1-1). The source of fluids for the gold mineralization of Tulu Kapi could be from intrusive events that emplaced the Kapi gabbro or the Dogi granite. The timing of metamorphism is 635 to 580 Ma (Ayalew et al., 1990). Therefore, magmatism or metamorphism could have been the source for fluids for the gold mineralization of Tulu Kapi, nonetheless, the ultimate source of the fluids remains unresolved.

2.9 Conclusions

- Gold mineralization at Tulu Kapi is hosted by a c. 738 Ma syenite along a splay of the regional Tuludimtu shear zone in the Western Ethiopian Shield.
- Mineralization in the Tulu Kapi syenite is structurally controlled.
- The orientation of stacked sub-horizontal en-echelon vein arrays, which are central to gold lodes, are consistent with having formed during reverse movement on the Bedele shear zone.
- Along the footwall of the syenite, at a three-way tectonic contact, a stockwork shoot is host to visible gold and intense alteration.

- Due to little deformation, the c. 700 Ma Kapi gabbro, which is intrusively juxtaposed to the east of the Tulu Kapi syenite, is host only to minor gold mineralization.
- The presence of coarse gold in the latest structures, V_3, but pre-orogenic collapse, points to gold mineralization occurring late in the area's deformation history.
- Greenschist-facies orogenic belts and trans-continental shear zones which cut across the Arabian Nubian Shield in Ethiopia appear to be analogous to globally typical host sites for orogenic gold deposits. Therefore, there is good geological potential for additional gold deposits in the southern portion of the shield.

Chapter 3 Conclusions and Future Research

3.1 General conclusions and implications for exploration

This MSc thesis project has advanced the understanding of the controls on gold mineralization in Tulu Kapi Gold Deposit. The controls on gold mineralization in the Tulu Kapi syenite can be used to guide the development of gold exploration models along the Tuludimtu shear zone. The deformational history of Tulu Kapi along with the U-Pb dates provided in this thesis can contribute to the further understanding of the southern Arabian Nubian Shield's tectonic history.

Kebede et al (1999) suggested that the Tulu Kapi syenite was post-tectonic. The conclusion of this thesis contradicts Kebede et al (1999), since the Tulu Kapi syenite is found to be pre-tectonic herein.

3.1.1 Controls on gold mineralization

The mineralization model provided by KEFI Minerals Plc. was tested and was found to fit into the structural model of shear controlled en-echelon vein arrays which were observed in outcrop and drill core. The reason for the location of these structures in the Tulu Kapi syenite is the rheologically distinct nature of the syenite as compared with the surrounding relatively more ductile lithological units (Figure 2-1). The crystalline Tulu Kapi syenite was competent and preferentially underwent brittle deformation, and these brittle structures served as fluid pathways during alteration and gold mineralization episodes.

3.1.2 Tulu Kapi proximate exploration

Tulu Kapi proximate exploration models should consider the structurally controlled nature of Tulu Kapi gold deposit and its location along the Bedele shear zone. Preliminary exploration in the proximity of Tulu Kapi should concentrate on lithological mapping along the Tuludimtu shear zone. The aim of the mapping should be to identify pre or syn-deformation plutonic rocks adjacent to the Tuludimtu shear zone or its splay shear zones and faults. Subsequent to the identification of intrusions, the second phase of exploration should include focused mapping of structural, lithological and alteration characteristics of the plutonic rocks along shear zones, accompanied by a chemical survey of rock chips from outcrop of the varied structural, lithological and alteration setting. The results of this second phase can then be used for more targeted exploration utilizing trenching.

The deep shoot in the Tulu Kapi gold deposit is a crunch-zone in the syenite. The continuity of the shoot down-plunge is likely, however its extent is not certain, since the structures which control the shoot and the lithology which hosts the shoot could terminate. Similar contacts in or near the gold deposit could be explored for. The recommended places to test for similar shoots would be along the Bedele shear zone where it intersects lithological and tectonic contacts.

3.1.3 Timing of gold mineralization and gold exploration

Mineralizaiton in Tulu Kapi is temporally constrained between the intrusions of the Kapi gabbro and the Genji granite. Dating intrusive rocks along the Tuludimtu belt is recommended during exploration, in order to focus on intrusive rocks which would have been exposed to sufficient deformation to host an abundance of structures like the c. 738 Ma Tulu Kapi syenite. The Kapi gabbro, c. 700 Ma, could be an example of a poorly mineralized intrusive rock along the Bedele shear zone, due to its late emplacement and thus limited exposure to deformation. While the Genji granite (c. 584 Ma; Blades et al., 2015), c. 584 Ma, could be an example of an unmineralized intrusive pluton along the Tuludimtu shear zone. While dating intrusive rocks along the Tuludimtu belt could identify post-deformation plutons, it should be used with caution as intrusions which crystallized late in the deformation history of the Tuludimtu shear zone, like the Kapi gabbro is presumed to have, could host economic mineralization.

3.2 Future research

3.2.1 Characterization of gold-bearing fluids

With the current understanding, fluids involved during the mineralization of the Tulu Kapi syenite could be either metamorphic or magmatic in origin. The determination whether gold-bearing fluids were metamorphic or magmatic in origin could assist with gold exploration in the proximity of the Tulu Kapi Gold Deposit. If the fluid source would be identified as magmatic, it could considerably assist with Tulu Kapi proximate exploration by utilising trace element zoning models (Goldfarb and Groves, 2015).

3.2.2 Determination of alteration fluid chemistry

Determination of the alteration fluid chemistry which resulted in the albite + silica + sulfide lodes in the Tulu Kapi syenite could assist with proximate exploration. Alteration assemblages could be

predicted in the lithologies along the Tuludimtu shear zone (e.g. Colvine et al., 1988). The pathway which the altering and gold mineralizing fluids took in Tulu Kapi syenite appears to be coincidental. If they are elsewhere as well in the Tulu Kapi proximity, then it could be used as an effective method of gold exploration through alteration mapping.

Bibliography

Alemu T., Abebe T., 2007. Geology and Tectonic Evolution of the Pan-African Tulu Dimtu Belt, Western Ethiopia. Online Journal of Earth Sciences 1, 24-42.

Allen A., Tadesse G., 2003. Geological setting and tectonic subdivision of the Neoproterozoic orogenic belt of Tuludimtu, western Ethiopia. Journal of African Earth Science 36, 329-343.

Ayalew T., Bell K., Moore J. M., and Parrish R. R., 1990. U-Pb and Rb-Sr geochronology of the Western Ethiopian Shield. Geological Society of America Bulletin, volume 102, 1309-1316.

Ayalew T., Peccerillo A., 1998. Petrology and geochemistry of the Gore-Gambella plutonic rocks: implications for magma genesis and the tectonic setting of the Pan-African Orogenic Belt of western Ethiopia. Journal of African Earth Sciences 27, 397-416.

Beach A., 1975. The geometry of en-echelon vein arrays. Tectonophysics, Vol. 28, 245-236.

Black L. P., Kamo S. L., Allen C. M. and Davis D. W., 2004. Improved 206Pb/238U microprobe geochronology by the monitoring of trace-element-related matrix effect: SHRIMP, ID-TIMS, ELA-ICP-MS and oxygen isotope documentation for a series of zircon standards. Chemical Geology, volume 205 (1-2), 115-140.

Blades M. L., Collins A. S., Foden J., Payne J. L., Xu X., Alemu T., Woldetinsae G., Clark C., Taylor R.J.M., 2015. Age and hafnium isotopic evolution of the Didesa and Kemashi Domains, western Ethiopia. Precambrian Research 270, 267-284.

Braathen A., Grenne T., Selassie M. G., Worku T., 2001. Juxtaposition of Neoproterozoic units along the Baruda – Tulu Dimtu shear-belt in the East African Orogen of western Ethiopia. Precambrian Research 107, 215-234.

Colvine A. C., Fyon J. A., Heather K. B., Marmont S., Smith P. M. and Troop D. G., 1988. Archean Lode Gold Deposits in Ontario. Ontario Geological Survey, Miscellaneous Paper 139.

Cox S. F., Etheridge M. A. and Wall V. J., 1986. The Role of Fluids in Syntectonic Mass Transport, and the Localization of Metamorphic Vein-Type Ore Deposits. Ore Geology Reviews, Volume 2, 65-86.

Craig J. R. and Vokes F. M., 1993. The metamorphism of pyrite and pyritic ores: and overview. Mineralogical Magazine, Volume 57, 3-18.

Fritz H., Abdelsalam M., Ali K. A., Bingen B., Collins A. S., Fowler A. R., Ghebreab W., Hauzenberger C. A., Johnson., P.R., Kusky T. M., Macey P., Muhongo S., Stern R. J., Viola G., 2013. Orogen styles in the East African Orogen: A review of the Neoproterozoic to Cambrian tectonic evolution. Journal of African Earth Sciences 86, 65-106.

Ghebreab W., Yohannes E., and Giorgis L. W., 1992. The Lega Dembi gold mine: an example of shear zone-hosted mineralization in the Adola greenstone belt, Southern Ethiopia. Journal of African Earth Sciences, Vol 15, No. ¾, 489-500.

Goldfarb R. J., Goves D. I. and Gardoll S., 2001. Orogenic gold and geologic time: a global synthesis. Ore Geology Reviews, volume 18, 1-75.

Goldfrab R. J. and Groves D. I., 2015. Orogenic gold: Common or evolving fluid and metal sources through time. Lithos, volume 233, 2-26.

Goldfarb R. J., Baker T., Dube B., Groves D. I., Hart C. J. R., Gosselin P., 2005. Distribution, Character, and Genesis of Gold Deposits in Metamorphic Terranes. Economic Geology 100th Anniversary Volume, 407-450.

Grenne T., Pedersen R. B., Bjerkgard T., Braathen A., Selassie M. G., Worku T., 2003. Neoproterozoic evolution of the Western Ethiopia: igneous geochemistry, isotope systematics and U-Pb ages. Geological Magazine 140: 373-395.

Groves D. I., Goldfarb R. J., Knox-Robinson C. M., Ojala J., Gardoll S., Yun G., and Holyland P., 2000. Late-kinematic timing of orogenic gold deposits and its significance for computer-based exploration techniques with emphasis on the Yilgarn block, Western Australi. Ore Geology Reviews, Volume 17, 1-38.

Groves D. I., Goldfrarb R. J., Robert F., and Hart C. J. R., 2003. Gold Depoists in Metamorphic Belts: Overview of Current Understanding, Outstanding Problems, Future Research, and Exploration Significance. Journal of Economic Geology, Volume 98, 1-29.

Hodgson J. C., 1989. The Structure of Shear-Related, Vein-Type gold Deposits: A Review. Ore Geology Reviews, Volume 4, 231-273.

Johnson T. E., Ayalew T., Mogessie A., Kruger F. J., Poujol M., 2004. Constraints on the tectonometamorphic evolution of the Western Ethiopian Shield. Precambrian Research 133, 305-327.

Johnson P. R., Andersen A., Collins A. S., Fowler A. R., Fritz H., Ghebreab W., Kusky T., Stern R. J., 2011. Late Cryogenian-Ediacaran history of the Arabian-Nubian Shield: A review of depositional, plutonic, structural, and tectonic events in the closing stages of the northern East African Orogen. Journal of African Earth Sciences 61, 167-232.

Johnson P. R., Zoheir B. A., Ghebreab W., Stern R. J., Barrie C. T., Hamer R. D., 2017. Gold-bearing volcanogenic massive sulfides and orogenic-gold deposits in the Nubian Shield. South African Journal of Geology, Vol 120.1, 63-76.

Kebede T., Koeberl C., Koller F., 1999. Geology, geochemistry and petrogenesis of intrusive rocks in the Wallagga area, western Ethiopia. Journal of African Earth Sciences 29, 715-134.

KEFI Minerals Plc. DFS, 2015: https://www.kefi-minerals.com/files/files/2015_TK_DFS_Complete_Final_Web.pdf. Site last accessed on 4 November 2018.

Olsen and Cleghorn, 2015. http://www.kefi-minerals.com/files/announcements/tulu_kapi_resource_update_04.02.15_1.pdf, site last accessed on 14 September 2017.

Paton C., Hellstrom J., Paul B., Woodhead J. and Hergt J., 2011. Iolite: Freeware for the visualisation and processing of mass spectrometric data. Journal of Analytical Atomic Spectrometry, volume 26, 2508-2518.

Phillips G. N. and Powell R., 2010. Formation of gold deposits: a metamorphic devolatilization model. Journal of Metamorphic Geology, volume 28, 689-718.

Poulsen K. H., Robert F. and Dubé B., 2000. Geological Classification of Canadian Gold Deposits. Geological Survey of Canada, Bulletin 540.

Ramsay J. G., 1967. Folding and fracturing of rocks. McGraw Hill, London.

Ramsay J. G. and Graham R. H., 1970. Strain variation in shear belts. Canadian Journal of Earth Science, Vol. 7, 786-813.

Robert F., Poulsen K. H., 2001. Vein formation and deformation in Greenstone gold deposits. Reviews in Economic Geology 14, Structural Controls on Ore Genesis Vol III, 111-180.

Sibson R. H., Robert F. K. and Poulsen H., 1988. High-angle reverse faults, fluid-pressure cycling, and mesothermal gold-quartz deposits. Geology, Volume 16, 551-555.

Slama J, Kosler J, Condon D. J., Crowley J. L., Gerdes A., Hanchar J. M., Horstwood M. S. A., Morris G. A., Nasdala L., Norberg N., Schaltegger U., Schoene B., Tubrett M. N. and Whitehouse M. J., 2008.Plesovice zircon – A new natural reference material for U-Pb and Hf isotopic microanalysis. Chemical Geology, volume 249, 1-35.

Stern R. J., 1994. Arc Assembly and Continental Collision in the Neoproterozoic East African Orogen: Implications for the Consolidation of Gondwanaland. Annual Reviews of Earth and Planetary Sciences 22, 319-351.

US Geological Survey, 2010. https://crustal.usgs.gov/geochemical_reference_standards/pdfs/STM-2.pdf. Site last accessed on 19 March 2019.

Vernon R. H., 2016. Rapakivi granite problems: plagioclase mantles and ovoid megacrysts. Australian Journal of Earth Sciences, volume 63, issue 6.

Wiedenbeck M., Alle P., Corfu F., Griffin W. L., Meier M., Oberli F, von Quadt A., Roddick J. C., Spiegel W., 1995. Three natural zircon standards for U-Th-Pb, Lu-Hf, trace element and REE analyses. Geostandards Newsletter, volume 19, 1-23.

Worku H., 1996. Structural control and metamorphic setting of the shear zone-related Au vein mineralization of the Adola Belt (southern Ethiopia) and its tectono-genetic development. Journal of African Earth Sciences, Vol. 23, No. 3, 383-409.

Yihunie T., Hailu F., 2007. Possible eastward tectonic collapse in the Arabian-Nubian shield of western Ethiopia. Journal of African Earth Sciences 49, 1-11.

Appendix A

Data of U-Pb zircon laser ablation ICP-MS geochronology

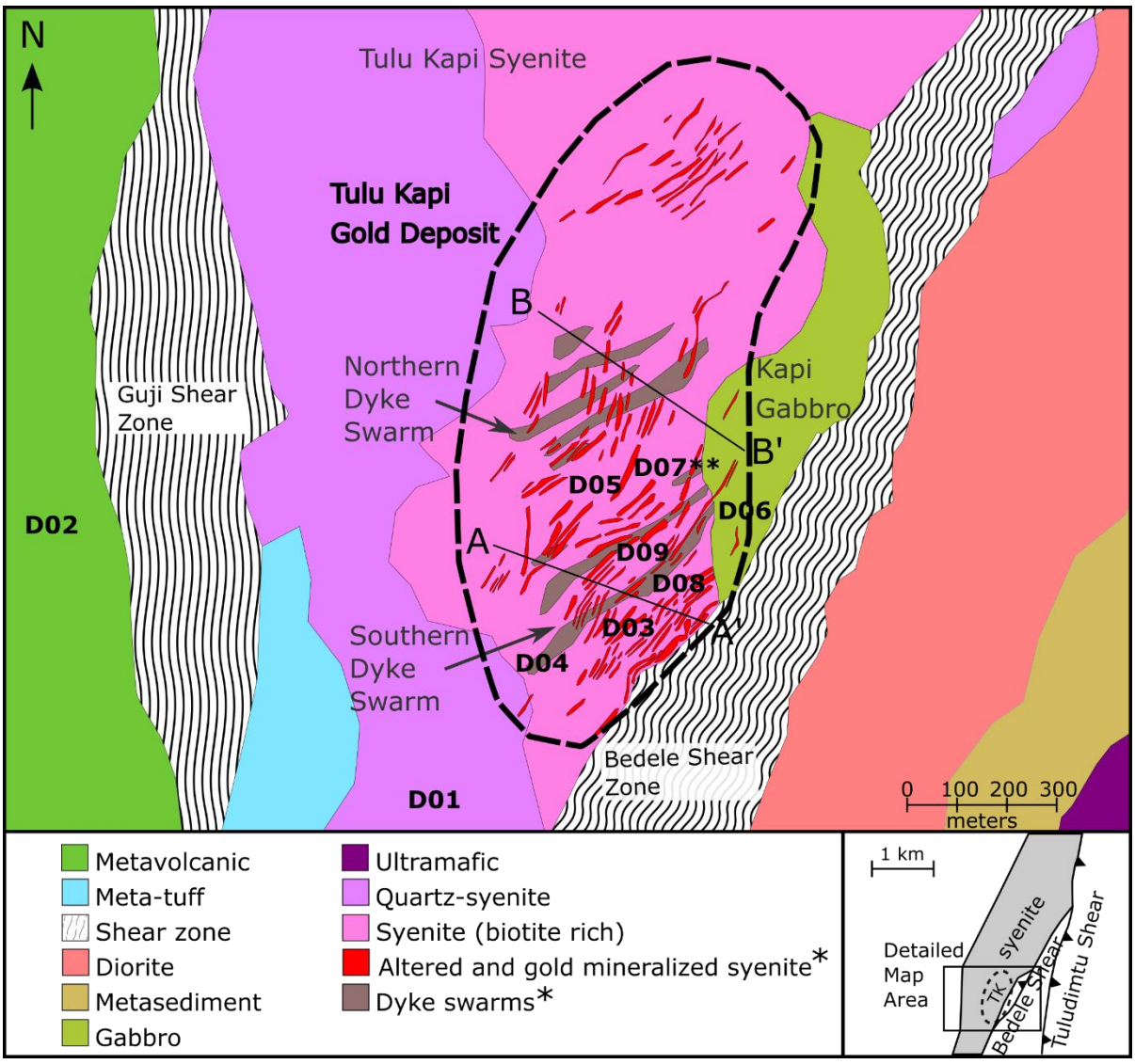

Figure 3-1: Local map of Tulu Kapi (modified after KEFI Minerals Ltd. DFS, 2015) with location of samples for U-Pb dating. ** Sample taken from trachyte below the Tulu Kapi syenite. * Dyke swarms and altered and gold mineralized syenite models are from historical models (KEFI Minerals Ltd. DFS, 2015). A-A' and B-B' are the locations of cross sections for Figure 2-10.

Table 3-1: U-Pb analyses sample summary table.

Sample ID	Rock Field Name	Source of sample
D01	Quartz syenite	Outcrop
D02	Metavolcanic	Outcrop
D03	Albitized syenite	Diamond drill-core
D04	Type-I dyke	Diamond drill-core
D05	Tulu Kapi syenite	Diamond drill-core
D06	Kapi Gabbro	Diamond drill-core
D07	Trachyte	Diamond drill-core
D08	Type-III dyke	Diamond drill-core
D09	Type-II dyke	Diamond drill-core

Isotope ratios

Sample	Lithology	Analysis	207Pb/235U	2SE	206Pb/238U	2SE	207Pb/206Pb	2SE
D01	Quartz syenite	D01-1.1	1.297	0.033	0.1225	0.0014	0.0724	0.0015
D01	Quartz syenite	D01-10.1	0.912	0.04	0.0832	0.003	0.0804	0.0013
D01	Quartz syenite	D01-11.1	1.136	0.021	0.1142	0.0012	0.0736	0.0014
D01	Quartz syenite	D01-12.1	1.095	0.023	0.1048	0.0023	0.0772	0.0014
D01	Quartz syenite	D01-13.1	1.176	0.021	0.1148	0.0012	0.0751	0.0012
D01	Quartz syenite	D01-14.1	1.118	0.02	0.1211	0.0016	0.0667	0.0011
D01	Quartz syenite	D01-15.1	1.056	0.016	0.116	0.0013	0.06528	0.00085
D01	Quartz syenite	D01-16.1	1.435	0.023	0.1154	0.0012	0.0875	0.0014
D01	Quartz syenite	D01-17.1	2.165	0.083	0.1271	0.002	0.1192	0.0037
D01	Quartz syenite	D01-18.1	1.119	0.023	0.1131	0.0017	0.0695	0.0012
D01	Quartz syenite	D01-19.1	1.126	0.021	0.1144	0.0013	0.0688	0.0012
D01	Quartz syenite	D01-2.1	0.774	0.019	0.0769	0.0026	0.0704	0.0012
D01	Quartz syenite	D01-20.1	4.75	0.31	0.1476	0.0038	0.233	0.012
D01	Quartz syenite	D01-21.1	2.316	0.099	0.1229	0.0015	0.1356	0.0058
D01	Quartz syenite	D01-22.1	1.389	0.06	0.1141	0.0016	0.0884	0.0036
D01	Quartz syenite	D01-23.1	1.305	0.021	0.1232	0.0014	0.0782	0.0012
D01	Quartz syenite	D01-24.1	1.452	0.037	0.1128	0.0016	0.0981	0.0023
D01	Quartz syenite	D01-25.1	1.03	0.026	0.1016	0.0022	0.077	0.0012
D01	Quartz syenite	D01-26.1	1.338	0.052	0.117	0.0016	0.0873	0.003
D01	Quartz syenite	D01-27.1	1.187	0.023	0.1197	0.0021	0.0756	0.0016
D01	Quartz syenite	D01-28.1	1.222	0.022	0.1168	0.0014	0.0776	0.0013
D01	Quartz syenite	D01-29.1	0.928	0.026	0.1027	0.0021	0.06621	0.00094
D01	Quartz syenite	D01-3.1	1.747	0.049	0.1324	0.0014	0.0905	0.0022
D01	Quartz syenite	D01-4.1	1.226	0.022	0.122	0.0015	0.0694	0.0012
D01	Quartz syenite	D01-5.1	1.099	0.017	0.1161	0.0017	0.06665	0.00096
D01	Quartz syenite	D01-6.1	1.104	0.019	0.1159	0.0017	0.0677	0.001
D01	Quartz syenite	D01-6.2	1.213	0.025	0.1264	0.0015	0.0681	0.001
D01	Quartz syenite	D01-7.1	1.245	0.034	0.1199	0.0013	0.074	0.0015
D01	Quartz syenite	D01-8.1	0.967	0.025	0.102	0.0021	0.0689	0.001

Appendix A continued

Isotope ratios

Sample	Lithology	Analysis	207Pb/235U	2SE	206Pb/238U	2SE	207Pb/206Pb	Sample
D01	Quartz syenite	D01-9.1	1.072	0.022	0.1171	0.0015	0.067	0.001
D02	Metavolcanic	D2-2.1	1.217	0.029	0.1288	0.0015	0.0687	0.0017
D02	Metavolcanic	D2-2.2	1.3	0.04	0.1298	0.0018	0.072	0.0021
D02	Metavolcanic	D2-3.1	1.111	0.027	0.1221	0.0015	0.066	0.0015
D02	Metavolcanic	D2-4.1	1.179	0.027	0.1271	0.0015	0.0668	0.0015
D02	Metavolcanic	D2-4.2	1.132	0.029	0.1246	0.0014	0.0647	0.0018
D02	Metavolcanic	D2-5.1	1.162	0.022	0.1248	0.0014	0.0681	0.0013
D02	Metavolcanic	D2-5.2	1.152	0.027	0.1222	0.0013	0.0679	0.0016
D02	Metavolcanic	D2-6.1	1.896	0.068	0.176	0.0033	0.0777	0.0028
D02	Metavolcanic	D2-7.1	0.225	0.038	0.01577	0.0008	0.099	0.017
D02	Metavolcanic	D2-7.2	0.136	0.019	0.01435	0.0007	0.074	0.013
D03	Albitized syenite	D03-1	1.065	0.029	0.1212	0.0031	0.0636	0.0012
D03	Albitized syenite	D03-10	1.116	0.026	0.1212	0.0024	0.0694	0.0012
D03	Albitized syenite	D03-11	1.643	0.051	0.1239	0.0025	0.0987	0.0022
D03	Albitized syenite	D03-12	7.51	0.72	0.1698	0.0073	0.311	0.014
D03	Albitized syenite	D03-13	7.8	1.3	0.174	0.011	0.294	0.025
D03	Albitized syenite	D03-14	1.59	0.12	0.1249	0.0034	0.0909	0.0044
D03	Albitized syenite	D03-15	1.08	0.023	0.1212	0.0024	0.0647	0.0013
D03	Albitized syenite	D03-16	4.58	0.28	0.1508	0.0043	0.2061	0.0083
D03	Albitized syenite	D03-17	1.094	0.025	0.1198	0.0023	0.0627	0.0013
D03	Albitized syenite	D03-18	2.389	0.099	0.131	0.0029	0.1246	0.0036
D03	Albitized syenite	D03-19	3.82	0.59	0.1395	0.0067	0.189	0.02
D03	Albitized syenite	D03-2	1.629	0.063	0.1267	0.0027	0.0916	0.0024
D03	Albitized syenite	D03-20	3.93	0.45	0.1454	0.0056	0.178	0.013
D03	Albitized syenite	D03-21	1.22	0.044	0.1232	0.0025	0.0705	0.0016
D03	Albitized syenite	D03-22	3.69	0.44	0.1421	0.0054	0.173	0.015
D03	Albitized syenite	D03-23	1.13	0.12	0.102	0.0068	0.0767	0.0032
D03	Albitized syenite	D03-24	2.088	0.093	0.129	0.0028	0.118	0.0039
D03	Albitized syenite	D03-25	4.45	0.38	0.1494	0.0041	0.212	0.013
D03	Albitized syenite	D03-26	1.244	0.065	0.1211	0.0025	0.0768	0.0037
D03	Albitized syenite	D03-27	7.1	0.28	0.1693	0.0039	0.3067	0.0065
D03	Albitized syenite	D03-28	2.74	0.46	0.1324	0.0054	0.132	0.012
D03	Albitized syenite	D03-29	1.61	0.11	0.124	0.0032	0.0925	0.0047
D03	Albitized syenite	D03-3	1.09	0.031	0.121	0.0027	0.0647	0.0015
D03	Albitized syenite	D03-30	1.088	0.027	0.1216	0.0024	0.0649	0.0012
D03	Albitized syenite	D03-31	2.268	0.082	0.1301	0.0027	0.125	0.0031
D03	Albitized syenite	D03-32	1.065	0.024	0.1189	0.0024	0.0645	0.0012
D03	Albitized syenite	D03-33	1.078	0.024	0.12	0.0023	0.0649	0.0012
D03	Albitized syenite	D03-34	1.579	0.049	0.1231	0.0027	0.0926	0.0021
D03	Albitized syenite	D03-35	1.089	0.029	0.1207	0.0027	0.0651	0.0014
D03	Albitized syenite	D03-36	1.344	0.036	0.1231	0.0025	0.0801	0.0018
D03	Albitized syenite	D03-37	1.065	0.028	0.1209	0.0026	0.0646	0.0013
D03	Albitized syenite	D03-38	1.101	0.025	0.1213	0.0024	0.0663	0.0013
D03	Albitized syenite	D03-39	3.65	0.31	0.1407	0.0046	0.182	0.011
D03	Albitized syenite	D03-4	1.086	0.028	0.1209	0.0029	0.0649	0.0014
D03	Albitized syenite	D03-40	1.078	0.031	0.1204	0.0025	0.0647	0.0015
D03	Albitized syenite	D03-41	1.066	0.029	0.1199	0.0025	0.0645	0.0014
D03	Albitized syenite	D03-42	2.3	0.18	0.1321	0.0031	0.1236	0.0069
D03	Albitized syenite	D03-43	1.134	0.021	0.1268	0.0015	0.0632	0.0011
D03	Albitized syenite	D03-44	1.12	0.024	0.1279	0.0017	0.0621	0.0012
D03	Albitized syenite	D03-45	1.168	0.023	0.1303	0.002	0.063	0.0013
D03	Albitized syenite	D03-46	1.125	0.02	0.1272	0.0016	0.0629	0.0011
D03	Albitized syenite	D03-47	1.57	0.043	0.1249	0.0026	0.0899	0.0016
D03	Albitized syenite	D03-48	3.207	0.083	0.1359	0.0025	0.1702	0.0025

Appendix A continued

Isotope ratios

Sample	Lithology	Analysis	207Pb/235U	2SE	206Pb/238U	2SE	207Pb/206Pb	Sample
D03	Albitized syenite	D03-49	1.071	0.021	0.1213	0.0023	0.0615	0.0012
D03	Albitized syenite	D03-5	2.14	0.2	0.1279	0.0033	0.1151	0.0065
D03	Albitized syenite	D03-50	1.068	0.021	0.1215	0.002	0.0615	0.0011
D03	Albitized syenite	D03-51	1.078	0.023	0.1216	0.0019	0.0621	0.0011
D03	Albitized syenite	D03-52	1.187	0.036	0.1225	0.0021	0.07	0.0028
D03	Albitized syenite	D03-53	1.045	0.022	0.1206	0.0019	0.0631	0.0012
D03	Albitized syenite	D03-54	1.022	0.022	0.1166	0.0021	0.0637	0.001
D03	Albitized syenite	D03-7	1.07	0.026	0.1193	0.0025	0.0698	0.0014
D03	Albitized syenite	D03-8	1.289	0.056	0.1225	0.0029	0.0801	0.0024
D03	Albitized syenite	D03-9	1.092	0.029	0.1198	0.0028	0.0698	0.0013
D04	Type-I dyke	D04-1	8.15	0.89	0.332	0.034	0.1616	0.0066
D04	Type-I dyke	D04-10	1.614	0.057	0.1594	0.0054	0.0747	0.0023
D04	Type-I dyke	D04-11.1	1.845	0.058	0.1838	0.0052	0.073	0.0019
D04	Type-I dyke	D04-11.2	1.101	0.053	0.1142	0.0048	0.0707	0.002
D04	Type-I dyke	D04-12	1.549	0.039	0.1573	0.0031	0.0729	0.0016
D04	Type-I dyke	D04-13	15	1.3	0.54	0.017	0.207	0.013
D04	Type-I dyke	D04-14	1.49	0.076	0.1469	0.0058	0.075	0.0032
D04	Type-I dyke	D04-15	1.503	0.069	0.1561	0.0056	0.0706	0.0023
D04	Type-I dyke	D04-16	7.21	0.21	0.3832	0.0098	0.1385	0.0023
D04	Type-I dyke	D04-17	0.967	0.085	0.0489	0.0013	0.145	0.012
D04	Type-I dyke	D04-18	2.303	0.074	0.1422	0.0039	0.1178	0.0026
D04	Type-I dyke	D04-19	4.08	0.2	0.191	0.01	0.1554	0.0034
D04	Type-I dyke	D04-2	1.158	0.03	0.1267	0.0032	0.065	0.0016
D04	Type-I dyke	D04-20	1.111	0.051	0.1068	0.0046	0.0746	0.0015
D04	Type-I dyke	D04-21	0.148	0.023	0.01525	0.0007	0.076	0.011
D04	Type-I dyke	D04-22	0.879	0.084	0.0928	0.0085	0.0671	0.0031
D04	Type-I dyke	D04-23	1.15	0.043	0.0985	0.0039	0.0829	0.0023
D04	Type-I dyke	D04-24	0.67	0.1	0.066	0.01	0.091	0.014
D04	Type-I dyke	D04-25	0.901	0.036	0.03841	0.0009	0.1731	0.0079
D04	Type-I dyke	D04-26	0.2941	0.008	0.03834	0.0007	0.0555	0.0011
D04	Type-I dyke	D04-27	0.155	0.051	0.0093	0.0026	0.135	0.073
D04	Type-I dyke	D04-28	3.07	0.11	0.2299	0.0068	0.0952	0.002
D04	Type-I dyke	D04-29	1.163	0.027	0.1262	0.0023	0.0652	0.0017
D04	Type-I dyke	D04-3.1	0.315	0.043	0.02737	0.0007	0.0792	0.0096
D04	Type-I dyke	D04-3.2	0.721	0.033	0.02653	0.0007	0.1853	0.0061
D04	Type-I dyke	D04-30	1.56	0.22	0.031	0.002	0.341	0.018
D04	Type-I dyke	D04-4	1.286	0.082	0.1322	0.0074	0.067	0.0021
D04	Type-I dyke	D04-5	0.638	0.028	0.0749	0.0024	0.0587	0.002
D04	Type-I dyke	D04-6_b	0.88	0.1	0.093	0.01	0.067	0.0048
D04	Type-I dyke	D04-7	1.576	0.056	0.1585	0.0038	0.0709	0.0024
D04	Type-I dyke	D04-8	0.633	0.038	0.0745	0.0022	0.0614	0.0037
D04	Type-I dyke	D04-9	1.243	0.043	0.1344	0.0035	0.0675	0.0023
D05	Tulu Kapi syenite	D05-1	1.16	0.019	0.125	0.0021	0.06666	0.00089
D05	Tulu Kapi syenite	D05-11	1.184	0.022	0.1292	0.0023	0.065	0.0011
D05	Tulu Kapi syenite	D05-12	1.024	0.014	0.1142	0.0017	0.06421	0.00099
D05	Tulu Kapi syenite	D05-13	1.107	0.028	0.1237	0.0022	0.0639	0.0015
D05	Tulu Kapi syenite	D05-14	1.099	0.022	0.1244	0.0016	0.0636	0.0012
D05	Tulu Kapi syenite	D05-15	1.401	0.086	0.1236	0.0021	0.0814	0.0048
D05	Tulu Kapi syenite	D05-16	1.068	0.021	0.1182	0.0017	0.0653	0.0012
D05	Tulu Kapi syenite	D05-17	1.181	0.02	0.1252	0.002	0.0685	0.001
D05	Tulu Kapi syenite	D05-18	1.079	0.019	0.1215	0.0019	0.0642	0.001
D05	Tulu Kapi syenite	D05-19	1.171	0.024	0.1317	0.0022	0.0645	0.0012
D05	Tulu Kapi syenite	D05-2	1.226	0.022	0.1294	0.0022	0.0677	0.001
D05	Tulu Kapi syenite	D05-20	0.926	0.029	0.0973	0.0021	0.0686	0.0012

Appendix A continued

Isotope ratios

Sample	Lithology	Analysis	207Pb/235U	2SE	206Pb/238U	2SE	207Pb/206Pb	Sample
D05	Tulu Kapi syenite	D05-21	1.159	0.017	0.1228	0.0017	0.06787	0.00091
D05	Tulu Kapi syenite	D05-22	1.169	0.021	0.1265	0.002	0.0665	0.0011
D05	Tulu Kapi syenite	D05-23	1.149	0.019	0.1249	0.0016	0.06602	0.00097
D05	Tulu Kapi syenite	D05-24	1.157	0.021	0.1284	0.0018	0.0644	0.0011
D05	Tulu Kapi syenite	D05-25	1.161	0.019	0.1285	0.0018	0.0654	0.0011
D05	Tulu Kapi syenite	D05-26	1.223	0.026	0.1241	0.002	0.0709	0.0012
D05	Tulu Kapi syenite	D05-27	1.1	0.023	0.1261	0.002	0.0634	0.0015
D05	Tulu Kapi syenite	D05-28	1.094	0.025	0.1254	0.002	0.0638	0.0015
D05	Tulu Kapi syenite	D05-29	1.059	0.021	0.1226	0.0023	0.0629	0.0013
D05	Tulu Kapi syenite	D05-3	1.185	0.052	0.1137	0.0025	0.0742	0.0023
D05	Tulu Kapi syenite	D05-30	1.168	0.036	0.1215	0.0023	0.0695	0.0019
D05	Tulu Kapi syenite	D05-31	1.058	0.02	0.1199	0.002	0.0639	0.001
D05	Tulu Kapi syenite	D05-32	1.106	0.041	0.1195	0.0025	0.0668	0.0022
D05	Tulu Kapi syenite	D05-34	1.39	0.042	0.1273	0.0022	0.0796	0.0026
D05	Tulu Kapi syenite	D05-35	1.161	0.022	0.1348	0.0021	0.0627	0.0011
D05	Tulu Kapi syenite	D05-36	1.308	0.036	0.1345	0.0024	0.0713	0.002
D05	Tulu Kapi syenite	D05-37	1.163	0.029	0.133	0.002	0.0632	0.0014
D05	Tulu Kapi syenite	D05-4	1.041	0.031	0.1111	0.0029	0.0668	0.0016
D05	Tulu Kapi syenite	D05-5	1.26	0.022	0.1381	0.0023	0.0666	0.0011
D05	Tulu Kapi syenite	D05-6	1.117	0.044	0.1013	0.0022	0.0769	0.0018
D05	Tulu Kapi syenite	D05-7	1.175	0.021	0.1319	0.0025	0.06425	0.00082
D05	Tulu Kapi syenite	D05-8	1.199	0.023	0.1345	0.0019	0.06446	0.00094
D05	Tulu Kapi syenite	D05-9	1.174	0.02	0.1301	0.0021	0.0648	0.001
D06	Kapi gabbro	D06-1.1	1.381	0.072	0.1155	0.0023	0.0861	0.0036
D06	Kapi gabbro	D06-10.1	1.73	0.11	0.1185	0.0025	0.1072	0.0064
D06	Kapi gabbro	D06-10.1-b	1.061	0.049	0.1169	0.0028	0.0661	0.0031
D06	Kapi gabbro	D06-11.1	1.16	0.042	0.1139	0.002	0.0733	0.0024
D06	Kapi gabbro	D06-12.1	1.102	0.035	0.1162	0.0022	0.0684	0.0021
D06	Kapi gabbro	D06-13.1	1.147	0.049	0.1163	0.0024	0.0714	0.0028
D06	Kapi gabbro	D06-14.1	1.072	0.029	0.1181	0.0021	0.0655	0.0015
D06	Kapi gabbro	D06-15.1	1.039	0.035	0.1179	0.0024	0.064	0.0022
D06	Kapi gabbro	D06-16.1	1.007	0.031	0.115	0.0021	0.0633	0.002
D06	Kapi gabbro	D06-17.1	1.047	0.029	0.1128	0.002	0.0675	0.0018
D06	Kapi gabbro	D06-18.1	1.266	0.061	0.1162	0.0027	0.0788	0.0035
D06	Kapi gabbro	D06-19.1	1.048	0.029	0.1157	0.0021	0.0656	0.0016
D06	Kapi gabbro	D06-2.1	2.024	0.073	0.1125	0.0021	0.1291	0.0043
D06	Kapi gabbro	D06-20.1	1.032	0.045	0.1146	0.0025	0.0649	0.0026
D06	Kapi gabbro	D06-21.1	1.025	0.029	0.1128	0.0022	0.0662	0.0019
D06	Kapi gabbro	D06-22.1	1.061	0.045	0.1121	0.0026	0.069	0.0027
D06	Kapi gabbro	D06-23.1	1.034	0.043	0.1151	0.0025	0.0656	0.0028
D06	Kapi gabbro	D06-24.1	1.081	0.044	0.1143	0.0025	0.0686	0.0028
D06	Kapi gabbro	D06-25.1	1.031	0.032	0.1134	0.0022	0.0654	0.0019
D06	Kapi gabbro	D06-26.1	1.327	0.087	0.1112	0.0025	0.0848	0.0042
D06	Kapi gabbro	D06-27.1	1.01	0.048	0.1138	0.0026	0.0644	0.0031
D06	Kapi gabbro	D06-28.1	1.144	0.065	0.1139	0.0029	0.0723	0.0038
D06	Kapi gabbro	D06-29.1	1.047	0.045	0.1155	0.0025	0.0653	0.0026
D06	Kapi gabbro	D06-3.1	1.068	0.028	0.1158	0.0022	0.066	0.0015
D06	Kapi gabbro	D06-30.1	1.027	0.039	0.1149	0.0025	0.0647	0.0024
D06	Kapi gabbro	D06-31.1	1.034	0.035	0.1141	0.0022	0.0656	0.0019
D06	Kapi gabbro	D06-32.1	1.041	0.037	0.1157	0.0022	0.065	0.0023
D06	Kapi gabbro	D06-33.1	0.993	0.031	0.1125	0.0022	0.0639	0.002
D06	Kapi gabbro	D06-34.1	1.38	0.12	0.1156	0.0029	0.0834	0.0047
D06	Kapi gabbro	D06-35.1	1.021	0.034	0.1124	0.0024	0.0661	0.0023
D06	Kapi gabbro	D06-36.1	1.056	0.029	0.1148	0.002	0.0664	0.0018

Appendix A continued

Isotope ratios

Sample	Lithology	Analysis	207Pb/235U	2SE	206Pb/238U	2SE	207Pb/206Pb	Sample
D06	Kapi gabbro	D06-37.1	1.069	0.03	0.1131	0.0019	0.0685	0.0016
D06	Kapi gabbro	D06-38.1	1.029	0.036	0.1141	0.0024	0.065	0.002
D06	Kapi gabbro	D06-39.1	1.284	0.057	0.1197	0.0026	0.0786	0.0033
D06	Kapi gabbro	D06-4.1	1.089	0.048	0.115	0.0026	0.0679	0.0027
D06	Gabbro	D06-40.1	1.134	0.053	0.1143	0.0025	0.0717	0.0029
D06	Gabbro	D06-41.1	1.003	0.049	0.116	0.003	0.0644	0.0035
D06	Gabbro	D06-42.1	1.135	0.049	0.1111	0.0021	0.0737	0.0028
D06	Gabbro	D06-5.1	1.161	0.068	0.1274	0.0031	0.0667	0.0039
D06	Gabbro	D06-6.1	1.183	0.051	0.1242	0.0024	0.0685	0.0028
D06	Gabbro	D06-6.1B	1.111	0.044	0.1157	0.0024	0.0717	0.0027
D06	Gabbro	D06-7.1	11.8	1.8	0.208	0.018	0.385	0.026
D06	Gabbro	D06-7.1B	1.022	0.046	0.1166	0.0027	0.0656	0.0032
D06	Gabbro	D06-8.1	3	0.17	0.1169	0.0029	0.188	0.011
D06	Gabbro	D06-8.1B	1.263	0.054	0.1182	0.0029	0.0773	0.0029
D06	Gabbro	D06-9.1	1.167	0.032	0.1191	0.0019	0.0705	0.0018
D06	Gabbro	D06-9.1B	1.067	0.031	0.1164	0.0025	0.0653	0.0018
D07	Trachyte	D7-1.1	0.1475	0.009	0.02028	0.0006	0.0543	0.004
D07	Trachyte	D7-10.1	0.1948	0.006	0.02151	0.0003	0.0653	0.002
D07	Trachyte	D7-11.1	1.213	0.025	0.1303	0.0016	0.067	0.0015
D07	Trachyte	D7-11.2	1.283	0.033	0.1284	0.0016	0.0725	0.0016
D07	Trachyte	D7-12.1	1.325	0.048	0.14	0.002	0.0678	0.0025
D07	Trachyte	D7-13.1	0.1541	0.005	0.02181	0.0003	0.0504	0.0019
D07	Trachyte	D7-13.2	0.141	0.009	0.02055	0.0004	0.0498	0.0034
D07	Trachyte	D7-15.1	0.443	0.027	0.03264	0.0008	0.0991	0.0061
D07	Trachyte	D7-15.2	0.286	0.013	0.02712	0.0007	0.0742	0.0033
D07	Trachyte	D7-16.1	0.538	0.021	0.0655	0.0011	0.059	0.0024
D07	Trachyte	D7-16.2	0.503	0.027	0.063	0.0011	0.0575	0.0031
D07	Trachyte	D7-17.1	0.412	0.011	0.05152	0.0009	0.0567	0.0012
D07	Trachyte	D7-17.2	0.507	0.011	0.0605	0.0012	0.0595	0.0012
D07	Trachyte	D7-18.1	1.089	0.033	0.1048	0.0039	0.0744	0.0015
D07	Trachyte	D7-2.1	1.136	0.033	0.1248	0.0021	0.0651	0.0019
D07	Trachyte	D7-2.2	1.169	0.04	0.1267	0.0019	0.0674	0.0024
D07	Trachyte	D7-3.1	1.193	0.045	0.1277	0.0018	0.0679	0.0026
D07	Trachyte	D7-4.1	1.186	0.036	0.1255	0.0018	0.068	0.002
D07	Trachyte	D7-5.1	1.148	0.033	0.1252	0.0019	0.0662	0.0019
D07	Trachyte	D7-5.2	1.176	0.03	0.1289	0.0016	0.0661	0.0017
D07	Trachyte	D7-6.1	0.672	0.031	0.0723	0.0011	0.0675	0.0031
D07	Trachyte	D7-7.1	1.153	0.047	0.127	0.0025	0.0658	0.0027
D07	Trachyte	D7-7.2	1.142	0.053	0.1257	0.0022	0.0656	0.0031
D07	Trachyte	D7-8.1	0.691	0.043	0.0732	0.0019	0.0679	0.0042
D07	Trachyte	D7-8.2	2.45	0.41	0.134	0.013	0.112	0.01
D07	Trachyte	D7-9.1	1.173	0.026	0.123	0.0018	0.0697	0.0019
D08	Type-III dyke	D8-1.1	1.08	0.015	0.1198	0.0013	0.06451	0.00093
D08	Type-III dyke	D8-10.1	1.016	0.012	0.1155	0.0013	0.06312	0.00063
D08	Type-III dyke	D8-11.1	0.865	0.093	0.0781	0.0075	0.078	0.0016
D08	Type-III dyke	D8-12.1	1.037	0.02	0.1143	0.002	0.0646	0.001
D08	Type-III dyke	D8-13.1	0.836	0.012	0.0951	0.0011	0.06304	0.00073
D08	Type-III dyke	D8-14.1	0.996	0.052	0.1128	0.0055	0.06332	0.00059
D08	Type-III dyke	D8-15.1	0.998	0.015	0.109	0.0015	0.06553	0.00078
D08	Type-III dyke	D8-16.1	1.132	0.021	0.1281	0.0013	0.0636	0.001
D08	Type-III dyke	D8-17.1	0.86	0.017	0.0954	0.0017	0.06519	0.00096
D08	Type-III dyke	D8-18.1	1.13	0.021	0.127	0.0016	0.0638	0.0012
D08	Type-III dyke	D8-19.1	0.98	0.012	0.1089	0.0012	0.06487	0.00076
D08	Type-III dyke	D8-2.1	1.552	0.089	0.1566	0.0065	0.07	0.0013

Appendix A continued

Isotope ratios

Sample	Lithology	Analysis	207Pb/235U	2SE	206Pb/238U	2SE	207Pb/206Pb	Sample
D08	Type-III dyke	D8-20.1	0.94	0.04	0.1049	0.0041	0.06467	0.00091
D08	Type-III dyke	D8-21.1	0.81	0.016	0.091	0.0019	0.06417	0.00081
D08	Type-III dyke	D8-22.1	1.058	0.015	0.1141	0.0011	0.06683	0.0009
D08	Type-III dyke	D8-23.1	0.891	0.011	0.0977	0.001	0.06573	0.00074
D08	Type-III dyke	D8-24.1	1.03	0.017	0.1127	0.0014	0.06587	0.00099
D08	Type-III dyke	D8-25.1	1.072	0.018	0.115	0.0012	0.06682	0.00098
D08	Type-III dyke	D8-26.1	1.097	0.016	0.1192	0.0014	0.06632	0.0009
D08	Type-III dyke	D8-27.1	1.052	0.017	0.1147	0.0015	0.0661	0.001
D08	Type-III dyke	D8-28.1	1.071	0.02	0.1152	0.0018	0.06655	0.00073
D08	Type-III dyke	D8-29.1	1.162	0.019	0.1221	0.0016	0.0667	0.0011
D08	Type-III dyke	D8-3.1	0.845	0.029	0.093	0.0031	0.06536	0.00086
D08	Type-III dyke	D8-30.1	0.926	0.057	0.0973	0.0054	0.0665	0.0013
D08	Type-III dyke	D8-31.1	1.204	0.018	0.127	0.0014	0.06698	0.0008
D08	Type-III dyke	D8-32.1	0.918	0.035	0.0954	0.0034	0.06783	0.00095
D08	Type-III dyke	D8-33.1	1.156	0.016	0.1193	0.0011	0.06839	0.00079
D08	Type-III dyke	D8-34.1	1.171	0.02	0.1221	0.0015	0.0684	0.0013
D08	Type-III dyke	D8-35.1	1.07	0.018	0.114	0.0013	0.0668	0.0012
D08	Type-III dyke	D8-36.1	1.097	0.018	0.1164	0.0018	0.0671	0.001
D08	Type-III dyke	D8-37.1	0.857	0.016	0.0923	0.0014	0.06559	0.00091
D08	Type-III dyke	D8-38.1	0.852	0.023	0.093	0.0022	0.0656	0.00085
D08	Type-III dyke	D8-39.1	1.151	0.019	0.1236	0.0015	0.0662	0.001
D08	Type-III dyke	D8-4.1	1.135	0.018	0.1266	0.0012	0.06492	0.00093
D08	Type-III dyke	D8-40.1	0.916	0.03	0.1002	0.0029	0.06626	0.00077
D08	Type-III dyke	D8-41.1	1.051	0.019	0.1164	0.0013	0.0657	0.0012
D08	Type-III dyke	D8-42.1	1.088	0.017	0.1183	0.0014	0.06676	0.00089
D08	Type-III dyke	D8-43.1	1.091	0.02	0.1221	0.002	0.06486	0.00096
D08	Type-III dyke	D8-44.1	1.142	0.018	0.1261	0.002	0.0658	0.0011
D08	Type-III dyke	D8-45.1	1.086	0.017	0.1209	0.0016	0.06553	0.00093
D08	Type-III dyke	D8-46.1	1.77	0.11	0.1274	0.0018	0.0997	0.0051
D08	Type-III dyke	D8-47.1	0.549	0.012	0.0634	0.001	0.06339	0.00084
D08	Type-III dyke	D8-5.1	1.029	0.03	0.1107	0.0029	0.06592	0.00093
D08	Type-III dyke	D8-6.1	0.951	0.039	0.1046	0.0035	0.0652	0.0012
D08	Type-III dyke	D8-7.1	1.138	0.018	0.1258	0.0016	0.06553	0.00095
D08	Type-III dyke	D8-8.1	1.093	0.018	0.121	0.0013	0.06485	0.00081
D08	Type-III dyke	D8-9.1	0.747	0.026	0.0841	0.0028	0.06356	0.00074
D09	Type-II dyke	D9-1.1	1.36	0.2	0.0462	0.003	0.199	0.017
D09	Type-II dyke	D9-10.1	1.103	0.017	0.1153	0.0022	0.0696	0.00096
D09	Type-II dyke	D9-11.1	1.157	0.053	0.1246	0.0021	0.0679	0.0035
D09	Type-II dyke	D9-11.2	1.17	0.059	0.1234	0.0029	0.0692	0.004
D09	Type-II dyke	D9-12.1	0.2042	0.01	0.02067	0.0003	0.0719	0.0032
D09	Type-II dyke	D9-13.1	1.402	0.02	0.1505	0.0017	0.06749	0.00067
D09	Type-II dyke	D9-14.1	1.295	0.035	0.1344	0.0021	0.0698	0.0013
D09	Type-II dyke	D9-15.1	0.54	0.048	0.0542	0.0042	0.0708	0.0016
D09	Type-II dyke	D9-16.1	1.19	0.021	0.1275	0.0015	0.0672	0.0011
D09	Type-II dyke	D9-17.1	0.275	0.016	0.03923	0.0009	0.0515	0.003
D09	Type-II dyke	D9-17.2	0.292	0.014	0.03839	0.0007	0.054	0.0023
D09	Type-II dyke	D9-2.1	0.641	0.046	0.03851	0.0008	0.1193	0.0082
D09	Type-II dyke	D9-3.1	22	4	0.313	0.038	0.474	0.038
D09	Type-II dyke	D9-4.1	1.38	0.1	0.0969	0.0058	0.1062	0.0037
D09	Type-II dyke	D9-5.1	1.14	0.021	0.1219	0.0024	0.06837	0.00084
D09	Type-II dyke	D9-6.1	3.29	0.31	0.204	0.016	0.1122	0.0034
D09	Type-II dyke	D9-7.1	1.094	0.095	0.0845	0.0024	0.0924	0.006
D09	Type-II dyke	D9-8.1	0.166	0.013	0.02083	0.0008	0.0571	0.0046
D09	Type-II dyke	D9-9.1	1.128	0.015	0.1227	0.0015	0.06681	0.00088

Appendix B

Lithogeochemistry Analysis Results

Table 3-2: Lithogeochemical analyses sample summary table. Sample locations as per Figure 3-1.

Sample ID	**Rock Field Name**	**Source of sample**
D01	Quartz syenite	Outcrop
D02	Metavolcanic	Outcrop
D03	Albitized syenite	Diamond drill-core
D04	Type-I dyke	Diamond drill-core
D05	Tulu Kapi syenite	Diamond drill-core
D06	Kapi Gabbro	Diamond drill-core
D07	Trachyte	Diamond drill-core
D08	Type-III dyke	Diamond drill-core
D09	Type-II dyke	Diamond drill-core
D10	Type-II dyke	Diamond drill-core. Duplicate of sample D09
D11	Syenite	Certified reference material (US Geological Survey, 2010).

Analyte Symbol	Au	As	Br	Cr	Ir	Sc	Se	Sb	Mass	SiO2	Al2O3
Unit Symbol	ppb	ppm	ppm	ppm	ppb	ppm	ppm	ppm	g	%	%
Detection Limit	2	0.5	0.5	5	5	0.1	3	0.2		0.01	0.01
Analysis Method	INAA	INAA	INAA	INAA	INAA	INAA	INAA	INAA	INAA	FUS-ICP	FUS-ICP
D_01	4	3.7	< 0.5	27	< 5	2.9	< 3	4	30.7	68.38	14.32
D_02	< 2	6.4	< 0.5	33	< 5	1.6	< 3	2.2	30.5	78.08	11.02
D_03	2100	208	< 0.5	< 5	< 5	4.7	< 3	0.8	31.1	66.11	13.61
D_04	82	11.5	< 0.5	27	< 5	11.1	< 3	1.9	31.6	60.49	13.61
D_05	15	6.3	< 0.5	19	< 5	6.8	< 3	0.7	32.8	63.37	14.47
D_06	< 2	10.1	< 0.5	64	< 5	34.1	< 3	4.3	31.3	48.83	14.68
D_07	< 2	17.3	< 0.5	19	< 5	8.5	< 3	2.2	30.6	65.31	15.94
D_08	< 2	15.8	< 0.5	42	< 5	23.5	< 3	0.9	30.8	54.6	14.28
D_09	4	7.5	< 0.5	49	< 5	23.4	< 3	0.8	31.9	52.34	15.05
D_10	< 2	9.4	< 0.5	47	< 5	22.4	< 3	0.7	31.3	52.89	15.74
D_11	< 2	12.2	< 0.5	21	< 5	1.1	< 3	< 0.2	1.47	60.04	17.98

Analyte Symbol	Fe2O3(T)	MnO	MgO	CaO	Na2O	K2O	TiO2	P2O5	LOI	Total
Unit Symbol	%	%	%	%	%	%	%	%	%	%
Detection Limit	0.01	0.001	0.01	0.01	0.01	0.01	0.001	0.01		0.01
Analysis Method	FUS-ICP	FUS-ICP	FUS-ICP	FUS-ICP	FUS-ICP	FUS-ICP	FUS-ICP	FUS-ICP	FUS-ICP	FUS-ICP
D_01	5	0.025	0.2	0.28	4.16	6.06	0.47	0.03	1.07	100
D_02	2.02	0.014	0.26	0.26	1.4	5.69	0.17	0.01	1.21	100.1
D_03	5.01	0.169	0.36	1.83	7.55	0.38	0.445	0.08	4	99.54
D_04	6.78	0.244	0.23	2.54	4.45	5.29	0.564	0.11	5	99.31
D_05	6.64	0.212	0.28	2.21	4.58	5.82	0.603	0.13	1.13	99.46
D_06	13.39	0.21	4.71	8.61	3.36	1.79	2.398	0.37	1.53	99.87
D_07	4.3	0.08	0.98	2.16	4.99	3.23	0.79	0.23	2.07	100.1
D_08	9.92	0.166	3.76	5.66	4.63	3.45	1.703	0.65	1.68	100.5
D_09	9.31	0.171	5.05	7.07	3.99	2.86	1.407	0.35	1.35	98.95
D_10	9.18	0.161	5.07	7.86	4.17	2.14	1.411	0.34	1.66	100.6
D_11	5.07	0.213	0.11	1.14	8.64	4.32	0.143	0.16	1.69	99.51

Analyte Symbol	Sc	Be	V	Cr	Co	Ni	Cu	Zn	Ga	Ge
Unit Symbol	ppm	ppm	ppm	ppm	ppm	ppm	ppm	ppm	ppm	ppm
Detection Limit	1	1	5	20	1	20	10	30	1	0.5
Analysis Method	FUS-ICP	FUS-ICP	FUS-ICP	FUS-MS	FUS-MS	FUS-MS	FUS-MS	FUS-MS	FUS-MS	FUS-MS
D_01	3	24	< 5	< 20	< 1	< 20	< 10	60	28	1.8
D_02	2	10	< 5	20	< 1	< 20	< 10	50	21	1.5
D_03	7	5	7	< 20	1	< 20	< 10	< 30	15	1.2
D_04	13	4	< 5	< 20	< 1	< 20	< 10	90	19	1.4
D_05	7	3	6	< 20	1	< 20	< 10	80	22	1.7
D_06	36	2	375	50	36	30	50	100	20	1.7
D_07	9	5	48	< 20	11	< 20	20	60	18	1.2
D_08	26	3	228	30	22	< 20	20	100	19	1.7
D_09	24	2	189	40	32	40	20	90	18	1.6
D_10	23	2	185	40	31	40	20	80	19	1.6
D_11	< 1	9	< 5	< 20	< 1	< 20	< 10	220	35	1.5

Analyte Symbol	As	Rb	Sr	Y	Zr	Nb	Mo	Ag	In	Sn
Unit Symbol	ppm	ppm	ppm	ppm	ppm	ppm	ppm	ppm	ppm	ppm
Detection Limit	5	1	2	0.5	1	0.2	2	0.5	0.1	1
Analysis Method	FUS-MS	FUS-MS	FUS-ICP	FUS-MS	FUS-ICP	FUS-MS	FUS-MS	FUS-MS	FUS-MS	FUS-MS
D_01	< 5	115	14	57.3	519	21.5	< 2	0.7	0.1	4
D_02	< 5	201	13	53.6	536	25.1	< 2	0.6	< 0.1	5
D_03	146	12	173	21.9	209	9.1	< 2	< 0.5	< 0.1	< 1
D_04	11	77	112	33.7	247	13.6	< 2	< 0.5	< 0.1	2
D_05	< 5	45	55	32	217	13.1	< 2	< 0.5	< 0.1	1
D_06	8	35	426	34.5	233	11.8	< 2	< 0.5	< 0.1	1
D_07	12	95	245	31	400	18.4	< 2	< 0.5	< 0.1	2
D_08	12	118	321	31.7	180	12	< 2	< 0.5	< 0.1	1
D_09	< 5	78	285	28.5	178	10.4	< 2	< 0.5	< 0.1	1
D_10	6	51	315	29.2	189	14.1	< 2	< 0.5	< 0.1	1
D_11	< 5	108	786	43	1177	201	6	1.5	< 0.1	6

Analyte Symbol	Sb	Cs	Ba	La	Ce	Pr	Nd	Sm	Eu	Gd
Unit Symbol	ppm	ppm	ppm	ppm	ppm	ppm	ppm	ppm	ppm	ppm
Detection Limit	0.2	0.1	2	0.05	0.05	0.01	0.05	0.01	0.005	0.01
Analysis Method	FUS-MS	FUS-MS	FUS-ICP	FUS-MS	FUS-MS	FUS-MS	FUS-MS	FUS-MS	FUS-MS	FUS-MS
D_01	3.6	2.4	109	68.7	149	18.9	74.1	15.7	1.07	12.8
D_02	1.7	2.7	54	34.3	69.3	8.28	30.9	6.75	0.197	6.88
D_03	0.7	0.4	83	18.6	40.3	5.21	21.7	5.66	3.79	5.33
D_04	1.6	0.5	541	26.8	56.8	6.86	27.4	6.26	2.27	5.99
D_05	0.5	1.8	977	24	52.7	6.8	28.4	6.22	3.45	6.03
D_06	4.1	1	1390	18.5	42.6	5.75	25.8	6.34	2.63	6.71
D_07	1.8	1.3	1821	38.8	77.6	8.98	33.6	6.57	1.7	5.9
D_08	0.8	6.3	470	33.6	73.8	9.07	38.3	7.96	2.42	7.13
D_09	0.6	2.8	412	20.9	45.4	5.6	23.1	5.55	1.76	5.67
D_10	0.5	1.9	349	21.1	44.7	5.47	23.9	5.37	1.77	5.55
D_11	0.5	1.3	653	154	263	25.3	79.4	12.4	3.42	8.85

Analyte symbol	Tb	Dy	Ho	Er	Tm	Yb	Lu	Hf	Ta	W
Unit Symbol	ppm	ppm	ppm	ppm	ppm	ppm	ppm	ppm	ppm	ppm
Detection Limit	0.01	0.01	0.01	0.01	0.005	0.01	0.002	0.1	0.01	0.5
Analysis Method	FUS-MS	FUS-MS	FUS-MS	FUS-MS	FUS-MS	FUS-MS	FUS-MS	FUS-MS	FUS-MS	FUS-MS
D_01	1.87	10.6	2.03	5.9	0.897	6.21	1.03	13.2	2.4	1.1
D_02	1.32	8.77	1.83	5.68	0.898	6.27	0.96	15.9	3.27	1
D_03	0.82	4.75	0.86	2.35	0.332	2.2	0.336	5.1	1.62	3520
D_04	0.98	5.85	1.16	3.46	0.522	3.57	0.572	6.7	1.98	280
D_05	0.95	5.82	1.11	3.35	0.485	3.57	0.52	5.6	1.81	37.9
D_06	1.06	6.43	1.21	3.31	0.478	3.07	0.468	6.2	1.63	18.2
D_07	0.88	5.24	1.04	3.07	0.452	3.14	0.508	10.2	2.03	15.8
D_08	1.09	6.08	1.14	3.05	0.419	2.79	0.379	4.6	1.68	10.6
D_09	0.87	5.08	1	2.79	0.423	2.69	0.393	4.9	1.29	7.9
D_10	0.9	5.39	1.03	2.79	0.42	2.79	0.392	5.1	3.47	7.2
D_11	1.43	7.97	1.46	4.17	0.606	4.06	0.597	28.1	16.5	5.1

Analyte Symbol	Tl	Pb	Bi	Th	U
Unit Symbol	ppm	ppm	ppm	ppm	ppm
Detection Limit	0.05	5	0.1	0.05	0.01
Analysis Method	FUS-MS	FUS-MS	FUS-MS	FUS-MS	FUS-MS
D_01	0.42	12	0.2	9.73	4.18
D_02	0.62	11	< 0.1	16.3	6.13
D_03	0.18	6	< 0.1	3.49	1.29
D_04	0.26	8	< 0.1	6.31	2.47
D_05	0.15	< 5	< 0.1	3.22	1.23
D_06	0.08	< 5	< 0.1	1.65	0.54
D_07	0.21	12	< 0.1	9.76	3.74
D_08	0.4	8	< 0.1	3.3	1.19
D_09	0.27	< 5	< 0.1	4.13	1.41
D_10	0.17	5	< 0.1	4.42	1.58
D_11	0.19	10	< 0.1	29	8.19